

Mathematical Modeling of Chemotaxis Guided Amoeboid Cell Swimming

Qixuan Wang^{1,2,*} and Hao Wu³

¹ Department of Mathematics, University of California, Riverside, CA, USA

² Interdisciplinary Center for Quantitative Modeling in Biology, University of California, Riverside, CA, USA

³ Department of Polymer Science and Engineering, University of Massachusetts, Amherst, MA, USA

* Author to whom any correspondence should be addressed.

E-mail: qixuanw@ucr.edu

December 2020

Abstract. Cells and microorganisms adopt various strategies to migrate in response to different environmental stimuli. To date, many modeling research has focused on the crawling-based *Dictyostelium discoideum* (Dd) cells migration induced by chemotaxis, yet recent experimental results reveal that even without adhesion or contact to a substrate, Dd cells can still swim to follow chemoattractant signals. In this paper, we develop a modeling framework to investigate the chemotaxis induced amoeboid cell swimming dynamics. A minimal swimming system consists of one deformable Dd amoeboid cell and a dilute suspension of bacteria, and the bacteria produce chemoattractant signals that attract the Dd cell. We use the *mathematical amoeba model* to generate Dd cell deformation and solve the resulting low Reynolds number flows, and use a moving mesh based finite volume method to solve the reaction-diffusion-convection equation. Using the computational model, we show that chemotaxis guides a swimming Dd cell to follow and catch bacteria, while on the other hand, bacterial rheotaxis may help the bacteria to escape from the predator Dd cell.

Keywords: Amoeboid cell swimming, chemotaxis, bacterial rheotaxis, finite volume method, low Reynolds number swimming, reaction-diffusion-convection equation.

1. Introduction

Cell migration, an integrated molecular process involving biochemical cascades intercorrelated with external chemical and mechanical stimuli, continues throughout the life span of many organisms [1]. Different microorganisms adopt various propulsion mechanisms and directed locomotion strategies for searching for food / running from predators. For example, individual cells and micro-organisms such as *C. reinhardtii* and spermatozoa find food by a combination of taxis and kinesis using a flagellated

or ciliated mode of swimming [2–5]. Other cell migration processes use the highly motile amoeboid mode, whose underlying molecular mechanisms have been extensively studied [6]. Amoeboid (e.g., *Dictyostelium discoideum* or leukocytes) cell migration relies on the generation, protrusion, and sometimes even travel of either pseudopodia or blebs [7]. As for strategies for directed locomotion, many flagellated bacteria (e.g., *E. coli*, *S. marcescens*, and *V. alginolyticus*) and even some eukaryotic organisms such as the green algae *C. reinhardtii* adopt a run- and-tumble type of motility [8]. During the run stage, the bacterium performs a more or less linear motion, while during the tumble stage it performs a highly erratic motion that produces little translocation but reorients the cell, thereby generating a random direction for the next run [9–11]. On the other hand, amoeboid cells detect extracellular chemical and mechanical signal gradients via membrane receptors, and these trigger signal transduction cascades that produce intracellular signals. Small differences in the extracellular signal are amplified into large end-to-end intracellular differences that control the motile machinery of the cell and thereby determine cell polarization and sites of pseudopod or bleb generation [12–18].

Due to their genetic, biochemical and cell-biological tractability, the social amoeba – *Dictyostelium discoideum* (Dd) have been a microorganism of choice to study basic processes in morphogenesis, including cell-cell chemical signaling, signal transduction, and cell motility [6, 19–22]. Crawling-based chemotaxis-driven Dd migration, at both individual and collective levels, has been well studied via both models and experiments [23–35]. To date, amoeboid cell migration and taxis are generally studied as the cells crawl on various solid substrates, relying on pseudopods attaching to the substrate. Recently, it was discovered that Dd cells can occasionally detach from the substrate and stay completely free in suspension for a few minutes before they slowly sink; during the free suspension stage, cells continue to form pseudopods that convert to rear-ward moving bumps, thereby propelling the cell through the surrounding fluid in a totally adhesion-free fashion [36]. Also, a mutant of Dd, *sadA*, which attaches poorly to a substrate, appears nevertheless to migrate normally and does so with an enhanced speed [37]. In the experiments, cells actively swam to a point source of cAMP, compared to no directed motion when the cAMP source is absent [37]. Furthermore, a similar adhesion-independent swimming model involving large-scale shape deformation of the cell body may be adopted by other cells, in particular, traditionally well known crawling cells: for example, human neutrophils swim to a chemoattractant fMLP (formyl-methionylleucyl-phenylalanine) source at a speed similar to that of cells migrating on a glass coverslip under similar conditions [37]. Most recently and equally striking, cytokine can induce *Drosophila* fat body cells to actively swim to wounds in an adhesion-independent motility mode associated with actomyosin-driven, peristaltic cell shape deformations that initiate from the cortex of the cell center and extend to the rear of the cell, propelling them forward. These waves occur constantly within fat body cells in unwounded pupae and become highly directed with respect to a wound. Once at the wound, fat body cells start to form lamellipodia that extend around the wound margin, assist hemocytes to clear the wound of cell debris, tightly seal the epithelial wound gap, and release

antimicrobial peptides to fight wound infection [38].

Inspired by these recent experimental discoveries of amoeboid mode of swimming – in the strict sense of adhesion-independent cell-fluid interaction that involves large-scale of cell shape deformations, it is timely to conduct a modeling study on chemotaxis driven Dd swimming that allows the coupling of signaling dynamics and biohydrodynamics. In recent years, several models for single cell amoeboid swimming have emerged, many focus on exploring the fluid-structure interaction in the system and how the amoeboid style of shape deformations lead to swimming in various viscous fluid environments [39–45], some also consider the underlying membrane protein kinetics that regulate the excitable dynamics of the the cell membrane deformations [46, 47]. In this paper, we develop a model that includes a deforming Dd amoeboid cell and a group of bacteria, where the amoeboid cell swims following chemoattractant signal produced by the bacteria. The model is a minimal one that couples the chemotaxis dynamics and the hydrodynamic effects. The paper is structured as follows. In section 2 we introduce the model setup, where the active bacterium motions are modeled by a random walk model (section 2.1), the chemotaxis signaling dynamics is numerically solved using the finite volume method in a moving mesh (section 2.2), the Dd amoeboid cell shape deformations and the resulting fluid dynamics are modeled and solved using an established complex analysis technique (section 2.3) [45, 48–50]. Numerical results are presented and discussed in section 3, where we first discussed the chemotaxis guided amoeboid swimming with one bacterium (section 3.1), then how bacterial rheotaxis could help the bacteria escape from the predator Dd cell (section 3.2), finally chemotaxis guided amoeboid swimming with a dilute suspension of bacteria (section 3.3).

2. Modeling framework

In this section we will discuss the development of the model, including the bacterial motions (section 2.1), the chemotaxis dynamics (section 2.2), the deforming Dd cell and the resulting fluid dynamics (section 2.3). We consider a system consisting of a Dd amoeboid cell and bacteria in low Reynolds number incompressible Newtonian fluid. For simplicity of modeling and computation, we will consider a 2D system. Many of the chemotaxis induced Dd cell swimming experiments are performed in containers sufficiently large so as to avoid influences from the walls [36, 37]. In this paper, we also consider a “large tank” modeling system, where the fluid mechanics resulted mainly from the swimming deformable Dd cells is obtained using the *mathematical amoeba model* [39, 45, 48–50] approach, which provides the solution in a 2D infinite fluid domain (section 2.3); on the other hand, the signaling dynamics is modeled using a moving-mesh based reaction-diffusion-convection (RDC) PDE model (section 2.2), where we assume a finite but sufficiently large computation domain for the RDC system. Such a coupled modeling framework allows us to efficiently study the dynamics of the system with relatively low computational costs, assuming the swimming Dd and bacteria are all away from the computational boundary of the RDC submodel.

2.1. Bacterium motions.

We consider *Escherichia coli* (*E. coli*) as a representative bacteria model. *E. coli*'s typical movement strategy is well known as run-and-tumble: an *E. coli* can either rotate its flagella counterclockwise resulting in a directed straight “run”, or rebundle its flagella by rotating them clockwise resulting in a “tumble” which reorients the cell without significant change of location [9, 10]. The *E. coli* constantly switch between the run and tumble modes. The mean run interval is reported to be about 1 sec in the absence of chemotaxis, and the mean tumble interval is about 0.1 sec, and both are distributed exponentially [11]. In our model system, we will first consider one amoeboid Dd cell with one *E. coli*, due to the small size of a *E. coli* (length $\sim 2 - 3\mu m$, diameter $\sim 1\mu m$ [51]) compared to that of a Dd cell (length $\sim 22 - 25\mu m$, diameter $\sim 4 - 6\mu m$ [36, 37]), the *E. coli* can be well modeled as moving particles without considering the flow stirred by their deformation and movement. Later (section 3.3) we will consider a system of one amoeboid Dd cell with a group of *E. coli* in a dilute suspension, where the number of *E. coli* is small (≤ 12) and are separated. In such a dilute suspension scenario, for simplicity, we do not consider the hydrodynamic effects among the *E. coli* or between the amoeboid Dd cell and a *E. coli*. However, we point out that if a large amount of *E. coli* is presented, the active suspension will greatly alter the hydrodynamic effects of the system, causing effects including clustering of *E. coli*. Refer to the Discussion section for potential future extensions.

We start with N_B bacteria in the system, where each bacterium is represented as a dot with its position vector $\mathbf{x}_n = (x_n, y_n)$, $n = 1, 2, \dots, N_B$. Without considering the flows generated by the movement of the bacteria, the movement of a bacterium mainly consists of two parts: a convection term of the fluid, and an active movement term from the run-and-tumble. Since the mean tumble interval (~ 0.1 sec) is much less than the mean run interval (~ 1 sec) [11], we model it as a random walk, where the run is modeled as a jump and the tumble serves a reorientation of the bacterium. The movement of each bacterium is described by the following equation:

$$d\mathbf{x}_n = \mathbf{u}(\mathbf{x}_n)dt + d\mathbf{X}_n \quad (1)$$

where $\mathbf{u}(\cdot)$ gives the fluid velocity field that is calculated via a complex analysis approach (section 2.3); \mathbf{X}_n denotes the random walk of the bacterium, and we assume that at each small time step dt , the bacterium moves a distance δ_J in the direction ϑ_n . In the following discussion we start by considering a 2D random walk of the bacterium, where $\vartheta_n \sim U(-\pi, \pi)$.

Recent research results reveal that bacterial rheotaxis plays a role in bacterial swimming, even without presence of a nearby surface [52]. To computationally investigate the effects of bacterial rheotaxis on bacterial escaping, that is, when the motions of the bacteria are directed in response to the local fluid velocity gradient, we use a hybrid type of random walk model to model the bacterial rheotaxis, where the moving direction ϑ_n is given by the following equation:

$$\vartheta_n = (1 - s_n)\xi_r \pm (\arg \mathbf{u}(\mathbf{x}_n) + s_n(1 - s_n)\pi\xi_b) \quad (2)$$

where $s_n = \min(1, \|\mathbf{u}(\mathbf{x}_n)\|/M) \in [0, 1]$ measures the sensitivity of the bacterium to the local fluid velocity with M the cut-off value for the fluid velocity amplitude. $\arg \mathbf{u}(\mathbf{x}_n)$ is the argument of the local fluid velocity, $\xi_r \sim U(-\pi, \pi)$ represents the random walk part of ϑ_n , $\xi_b \sim N(0, 1)$ and the sum of the two terms ($\arg \mathbf{u}(\mathbf{x}_n) + s_n(1 - s_n)\pi\xi_b$) represents the correlation with the fluid velocity due to rheotaxis, where we assume two types of rheotactic movement – along the flow (+) or against it (–). Equation (2) is an empirical way to model the bacterial rheotaxis, in a way to ensure that 1) when the bacterium is far apart from the Dd cell ($s_n \rightarrow 0$), the bacterium does not sense the flow thus it undergoes a random walk without bias (notice that with $\xi_r \sim U(-\pi, \pi)$, we have $\xi_r \pm \Theta \sim U(-\pi, \pi)$ for any angle Θ), 2) when the bacterium is near the Dd cell ($s_n \rightarrow 1$), bacterial movement is dominated by rhotaxis ($\vartheta_n = \pm \arg \mathbf{u}(\mathbf{x}_n)$), and 3) bacterial movement continuously change between unbiased and biased random walk depending on s_n .

Comparing to a typical shape deformation cycle of a Dd cell of about $T \sim 1 - 2$ min [36, 37], the mean run interval is ~ 1 sec subjected to exponential distribution [11]. For simplicity, we take the small time step dt of the random walk $d\mathbf{X}_n$ as $dt = 0.1T$, where T is the average period of a Dd cell swimming cycle.

2.2. Chemotaxis signaling dynamics.

Dictyostelium discoideum (Dd) utilizes folic acid receptor 1 (fAR1), a class of single G-protein-coupled receptor (GPCR) to detect diffusible chemoattractant folate secreted by bacteria, thus to locate and chase bacteria [53]. Once the amoeba “catches” the bacteria, the amoeba engulfs and consumes them. Dd amoeboid cell is reported to ingest, kill and digest bacteria at a rate of at least one per minute [54].

Suppose that at time t , the amoeboid cell captures a region $\Omega_{\text{Dd}}(t)$ in the 2D infinite domain, thus Ω_{Dd}^C , $\partial\Omega_{\text{Dd}}$ give the external fluid domain and the cell boundary, respectively. Let $f(\mathbf{x}, t)$, $R_f^0(\mathbf{x}, t)$ and $R_f(\mathbf{x}, t)$ denote the concentration of diffusive folate, the surface concentration of free fAR1 receptors and the surface concentration of the folate-bound fAR1 receptors, respectively. $f(\mathbf{x}, t)$ is defined on $\Omega_{\text{Dd}}^C(t) \times [0, \infty)$ and $R_f^0(\mathbf{x}, t)$, $R_f(\mathbf{x}, t)$ are defined on $\partial\Omega_{\text{Dd}}(t) \times [0, \infty)$. The signaling dynamics of the diffusible chemoattractant folate and the fAR1 receptors on the cell membrane are modeled by the following reaction-diffusion-convection (RDC) equations together with boundary conditions:

$$\frac{\partial f}{\partial t} = D\Delta f - \mathbf{u} \cdot \nabla f + a \int \sum_{n=1}^{N_B} \delta(\mathbf{x} - \mathbf{x}_n) d\mathbf{x} \quad \text{in } \Omega_{\text{Dd}}^C(t) \quad (3)$$

$$D \frac{\partial f}{\partial n} = -k_+ f R_f^0 + k_- R_f \quad \text{on } \partial\Omega_{\text{Dd}}(t) \quad (4)$$

$$\frac{\partial R_f}{\partial t} = k_+ f R_f^0 - k_- R_f - \gamma R_f + \varsigma R_f \frac{dW}{dt} \quad \text{on } \partial\Omega_{\text{Dd}}(t) \quad (5)$$

with the constraints:

$$R_f^0(\mathbf{x}, t) + R_f(\mathbf{x}, t) = R_{\max}, \quad f(\mathbf{x}, t) \geq 0, \quad R_f^0(\mathbf{x}, t) \geq 0, \quad R_f(\mathbf{x}, t) \geq 0$$

The terms in equations (3 - 5) are explained as follows.

- $D\Delta f$: diffusion of folate with the diffusion rate D .
- $\mathbf{u} \cdot \nabla f$: convection of folate, where \mathbf{u} gives the velocity field of the extra-cellular flow.
- $a \int \sum \delta d\mathbf{x}$: production of folate molecules from the bacteria, where a is the folate production rate. For simplicity, we assume that all bacteria have the same folate production rate.
- $k_+ f R_f^0, k_- R_f$: biochemical reactions between folate molecules and fAR1 receptors along the cell membrane boundary, where k_+, k_- are the binding and unbinding rates of the fAR1 receptors. R_{\max} is the sum of free and folate-bound receptors, and we assume it a constant along the cell boundary.
- γR_f : degradation of folate-bound fAR1 receptors, where γ is the degradation rate.
- $\varsigma R_f dW$: white noise that captures stochastic effects in intracellular signal dynamics, where ς is the noise strength.

Computationally, instead of considering the infinite fluid domain, we consider a finite but large enough computational domain Ω_{Chem} that contains the cell domain Ω_{Dd} and all the bacteria, and $\text{Area}(\Omega_{\text{Dd}}) \ll \text{Area}(\Omega_{\text{Chem}})$ (illustrated in figure 1A). Therefore the fluid domain boundary consists of two pieces: $\partial\Omega_{\text{Dd}}$ and $\partial\Omega_{\text{Chem}}$. We assume no-flux Neumann boundary condition $\hat{\mathbf{n}} \cdot \nabla f = 0$ on $\partial\Omega_{\text{Chem}}$.

To solve the RDC equations (3-5), we use the Voronoi tessellation based finite volume method formulated in [55, 56]. Initially, we generate a network of fluid “nodes” $\{\mathbf{w}_i\}$ in the computational fluid domain $\Omega_{\text{Chem}} \cap \Omega_{\text{Dd}}^C$, and discretize the cell boundary $\partial\Omega_{\text{Dd}}$ by N_R nodes $\mathbf{w}'_0, \mathbf{w}'_1, \dots, \mathbf{w}'_{N_R} = \mathbf{w}'_0$ - how to choose the discretization will be discussed in section 2.3. Notice that the positions of both the boundary nodes $\{\mathbf{w}'_i(t)\}$ and $\{\mathbf{w}_i(t)\}$ change as the Dd cell deforms and perturbs the surrounding fluid. At each computational time step, the fluid nodes $\{\mathbf{w}_i\}$ are updated as

$$\mathbf{w}_i^{n+1} = \mathbf{w}_i^n + \mathbf{u}(\mathbf{w}_i^n) \Delta t \quad (6)$$

where \mathbf{u} is the fluid velocity field. We generate a Voronoi tessellation $\{V_i^{n+1}\} \cup \{V_i^{m+1}\}$ of the computational domain $\Omega_{\text{Chem}} \cap \Omega_{\text{Dd}}^C$ based on the nodes $\{\mathbf{w}_i^{n+1}\} \cup \{\mathbf{w}_i^{m+1}\}$, that is, V_i^{n+1} (or V_i^{m+1}) is the set of all the points in the computational fluid domain $\Omega_{\text{Chem}} \cap \Omega_{\text{Dd}}^C$ closer to the node \mathbf{w}_i (or \mathbf{w}'_i) than any other node (figure 1B).

The folate concentration data f is available at the nodes $\{\mathbf{w}_i\}$. In the Lagrangian frame, the convection term $\mathbf{u} \cdot \nabla f$ disappears from equation (3). The Laplacian in equation (3) can thus be approximated for each Voronoi tile V_i through summation of the fluxes across the edges partitioning V_i from each of its Delaunay neighbors (denoted by Λ_i) [55]:

$$\Delta f_i \approx \frac{1}{\text{Area}(V_i)} \int_{\partial V_i} \mathbf{n} \cdot \nabla f ds \approx \frac{1}{\text{Area}(V_i)} \sum_{j \in \Lambda_i} \frac{f_j - f_i}{\|\mathbf{w}_j - \mathbf{w}_i\|} l_{ij} \quad (7)$$

where $f_i = f(\mathbf{w}_i)$, and l_{ij} is the length of the common edge shared by V_i and V_j . Notice that for a Voronoi tile V_i , its Delaunay neighbors may also include Dd cell boundary tiles

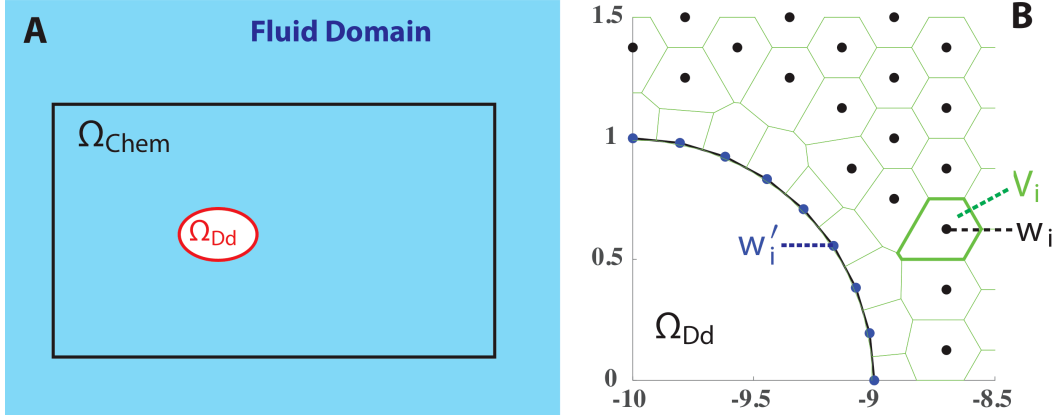


Figure 1: **A** Illustration of the geometry of the computational domains. **B** A local view of the Voronoi meshes near the Dd cell.

V'_i , but for simplicity, we omit the notation ' in equation (7). Numerical convergence studies show that the method converges linearly in the L^2 norm [57]. We solve equations (3) numerically in a forward Euler scheme, with the Laplacian approximated by equation (7). Equation (3) can be numerically solved as follows:

$$f_i^{n+1} = f_i^n + \left(D\Delta f_i^n + \frac{a \sum_{n=1}^{N_B} \delta_{V_i}(\mathbf{x}_n)}{\text{Area}(V_i)} \right) \Delta t$$

where $\delta_{V_i}(\mathbf{x}_n) = 1$ if the n th bacteria is in V_i , otherwise $\delta_{V_i}(\mathbf{x}_n) = 0$.

For boundary conditions, first we notice that while other nodes \mathbf{w}_i locates inside the corresponding Voronoi tile V_i , the cell boundary nodes \mathbf{w}'_i locate on $\partial V'_i \cup \partial \Omega_{Dd}$ (figure 1B). To each cell boundary \mathbf{w}'_i , the numerical Laplacian equation (7) can be modified as:

$$\Delta f_i \approx \frac{1}{\text{Area}(V'_i)} \left(\sum_{j \in \Lambda_i} \frac{f_j - f_i}{\|\mathbf{w}_j - \mathbf{w}'_i\|} l_{ij} + (\mathbf{n} \cdot \nabla f) l'_i \right) \quad (8)$$

where we approximate the boundary $\partial V_i \cap \partial \Omega_{Dd}$ by a line segment connecting the two vertices shared by neighboring Voronoi tiles, and let l'_i be its length. For boundary condition on $\partial \Omega_{Dd}$ given by equation (4), along the small boundary segment $\partial V'_i \cap \partial \Omega_{Dd}$ we have:

$$\frac{\partial f}{\partial n} = \mathbf{n} \cdot \nabla f = \frac{1}{D} (-k_+ f R_f^0 + k_- R_f)$$

and equation (8) becomes:

$$\Delta f_i \approx \frac{1}{\text{Area}(V_i)} \left(\sum_{j \in \Lambda_i} \frac{f_j - f_i}{\|\mathbf{w}_j - \mathbf{w}'_i\|} l_{ij} + \frac{l'_i}{D} (-k_+ f R_f^0 + k_- R_f) \right)$$

Finally, the no-flux boundary condition on $\partial \Omega_{Chem}$ can be directly enforced to equation (8).

2.3. Chemotaxis induced Dd shape deformations and swimming.

When adhesion is absent thus cell crawling is disabled, Dd cells can swim towards a chemoattractant source. During swimming, cells form pseudopods that convert to rearward moving bumps thereby propelling itself through the surrounding fluid in a totally adhesion-free fashion [7, 36, 37, 58]. Such a swimming mode is very different from ciliated or flagellated swimming modes that are commonly adopted by many bacteria including *E. coli*, as it is the one that requires large deformations that propagate over the cell body. We use the *mathematical amoeba model* [39, 45, 48–50] to generate the Dd cell deformation as well as to solve the resulting cell-fluid interaction. In the following we list the outline of the modeling framework, see the Appendix for more details.

Consider the following conformal mapping defined from $\{\zeta \in \mathbb{C}; |\zeta| \geq 1\}$ to Ω_{Dd}^C :

$$w(\zeta; t) = e^{i\theta(t)} \left[r(t)\zeta + \frac{\eta_{-1}(t)}{\zeta} + \frac{\eta_{-2}(t)}{\zeta^2} \right] + Z_{\text{Dd}}(t) \quad (9)$$

where the Dd cell shape is defined by $\partial\Omega_{\text{Dd}}(t) = \{w(\sigma; t) | \sigma \in S^1\}$. The N_r discretization nodes $\{\mathbf{w}'_1, \mathbf{w}'_2, \dots, \mathbf{w}'_{N_r}\}$ are generated as follows: we discretize the unit circle ∂D in the computational ζ -plane equally into N_r nodes:

$$\sigma_j = e^{i\theta_j} = e^{i\frac{2\pi j}{N_r}}, \quad j = 0, 1, 2, \dots, N_r - 1$$

then let $\mathbf{w}'_j = w(\sigma_j; t)$. In Eq (A.9), $\theta(t) \in \mathbb{R}$ gives the cell polarization that will be determined by signaling sensing dynamics as discussed below. The swimming Dd cell undergoes cyclic shape deformation with the same period T . We assume that the polarization θ is determined at the beginning of a swimming cycle and will not change during the cycle, thus $\theta(nT + t) \equiv \theta(nT)$ for $t \in [0, T)$. $r, \eta_{-1}, \eta_{-2} \in \mathbb{R}$ control the cell size and shape deformations, and are subjected to area conservation of the cell. $Z_{\text{Dd}}(t)$ gives the location of the cell, while $U_{\text{Dd}}(t) = \dot{Z}_{\text{Dd}}(t)$ gives the velocity of the cell and is computed from the Goursat formula [59]. The fluid velocity field \mathbf{u} , or in the complex notation u , can be also obtained through the Goursat formula. Refer to Appendix A for more details of the complex analysis techniques involved in this part.

We assume that the Dd cell undergoes shape deformations in response to signal gradient, with each swimming cycle lasting for a period of T and consisting of three phases: (i) *polarization*, when the Dd cell determines the polarization θ during the current cycle in response to the signal R_f , and elongates its cell body in preparation for (ii) *swimming*, when the Dd cell deforms its shape so to actively swim along the polarization direction, followed (iii) *relaxation*, when the Dd cell returns to its initial circular shape. Durations of polarization and relaxation phases are chosen to be much shorter than the swimming phase. Figure 2 shows a typical cycle of the Dd cell shape deformations. For more details of the modeling setup of the signaling induced Dd cell polarization and shape deformations, please refer to Appendix B.

In our model, we do not model the engulfment process in phagocytosis. For simplicity, once a bacterium falls within a close enough distance near a cell boundary node \mathbf{w}'_j , we consider it taken by the amoeba and remove it from the system.

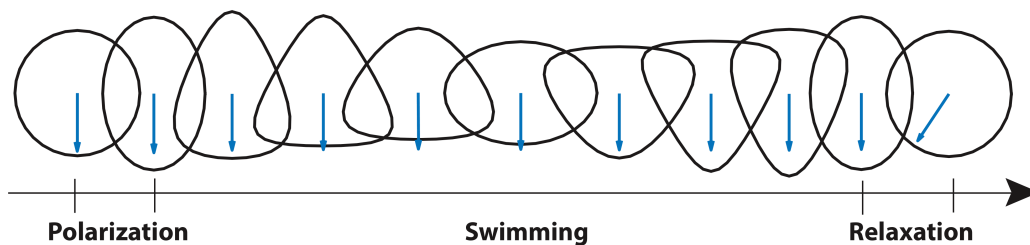


Figure 2: Shapes of the Dd cell in a cycle, showing the polarization, swimming and relaxation phases. Arrows indicate the cellular polarization direction θ within the cycle. At the end of the cycle, a new direction is selected.

2.4. Computations of the model

We nondimensionalize the system, using the duration of a Dd cell swimming cycle T and the radius of a Dd cell at rest r_0 as the characteristic temporal and spatial scales, and R_{\max} the characteristic concentration scale for f and R_f . The non-dimensionalized system can be found in Appendix C.

The system is computed using the following update algorithm:

- (i) **Signaling dynamics.** Generate the Voronoi tessellation from the current distribution of “nodes” $\{\mathbf{w}_i\} \cup \{\mathbf{w}'_i\}$. Update f and R_f by solving the RDC equations using the finite volume method in the moving mesh.
- (ii) **Dd amoeboid cell shape.**
 - **If** the cell is at rest in a circular shape ($t = nT$, $n \in \mathbb{N}$), determine the cell polarization θ for this swimming cycle.
 - **ElseIf** the cell is during a swimming cycle, $t \in (nT, (n+1)T)$, $n \in \mathbb{N}$, update the conformal mapping w equation (A.9).
- (iii) **Fluid mechanics.** Update flow velocity field \mathbf{u} from the Goursat formulas. Update bacteria positions and the moving mesh:
 - **Bacteria motions.** Update bacterial positions by equation (1). Remove any bacterium that comes to cell boundary Voronoi tiles.
 - **Moving mesh.** Update the moving mesh nodes $\{\mathbf{w}_i\}$ from equation (6).

The numerical scheme works for our model system where hydrodynamics and signaling dynamics are coupled, and allows us to study cellular chemotaxis and rheotaxis in a fluid environment. We point out that we do see fluid nodes near the Dd cell boundary getting closer after many swimming cycles due to the large deformation of the cell, which causes numerical instability of the finite volume method. We solve this numerical issue by a local re-mesh near the Dd cell, see more details in Appendix D. Parameter values used in our simulations are given in Table E1.

3. Results

3.1. Chemotaxis guided amoeboid swimming allows the Dd amoeboid cell to follow and catch bacteria

We start with a system consisting of one Dd cell and one bacterium where the bacterium undergoes an unbiased random walk (equation (1)). Simulation results show that the Dd amoeboid cell is able to swim following the bacterium guided by the chemoattractant signal. Figure 3 shows a typical simulation, where the Dd cell catches the bacterium after 69 cycles. Compared to the random walk of the bacterium, the motion of the Dd cell is more directed; as the Dd cell approaches the bacterium, the bacterium is pushed away to the right by the flow generated by the swimming Dd cell, and eventually being captured by the Dd cell (figure 3C). The full time lapse snapshots of the fluid velocity profile during one Dd cell swimming cycle is provided in Figure F1.

We consider how the chemoattractant diffusion rate D and the bacterial jump amplitude δ_J affect the Dd cell swimming dynamics. We perform 6 groups of 10 simulations, with different values of D and δ_J : $D = 0.2, 0.5, 1, \delta_J = 0.02, 0.1$. Simulation results show large coefficient rate D makes it easier for the Dd cell to follow the signal guidance thus catch the bacterium; bacterial random walk strength δ_J may also help the bacterium to escape, however, the more important effect of δ_J is that it increases the variance of time for the Dd cell to catch the bacterium, if it could (figure 4). The increase of catch time variance needed caused by δ_J should not be surprising, since the passive motion of the bacterium is an unbiased random walk \mathbf{X} , thus $E(\mathbf{X}) = 0$ and large δ_J only increases $\text{Var}(\mathbf{X})$ which in return increases the catch time variance, though through a complex chemotaxis induced amoeboid swimming dynamics. Figure 4 shows that in 10 out of 10 simulations with $D = 0.5, \delta_J = 0.02$ (figure 4C) $D = 1, \delta_J = 0.02$ (figure 4C) or $D = 1, \delta_J = 0.1$ (figure 4F), the Dd cell is able to catch the bacterium within 300 cycles, compared to 9 out of 10 with $D = 0.2, \delta_J = 0.02$ (figure 4A) and 7 out of 10 with $D = 0.5, \delta_J = 0.1$ (figure 4E). The worst scenario for the Dd cell is small D and large δ_J : with $D = 0.2, \delta_J = 0.1$, only in 2 out of 10 simulations the Dd cell catches the bacterium within 300 cycles (figure 4D). In the above simulations we take $k_- = 0$, finally we take $k_- = 0.1$ and with $D = 0.5, \delta_J = 0.02$, the results from 10 simulations are shown in Figure F2, compare with $k_- = 0$ (figure 4B), which indicates that large k_- helps the bacterium to escape from the Dd cell.

We present the time lapse snapshots from typical simulations with $\delta_J = 0.1, D = 0.2, 0.5, 1$ in Figures F3 - F5.

3.2. Rheotaxis helps bacteria escaping from the predator

Next, we use the model to investigate if rheotaxis could help the bacterium run away from the predator Dd cell. In particular, we consider two types of bacterial rheotaxis: the bacterium prefers to move with the flow vs. against the flow. We model either of the two rheotactic systems by a biased random walk of the bacterium, where the

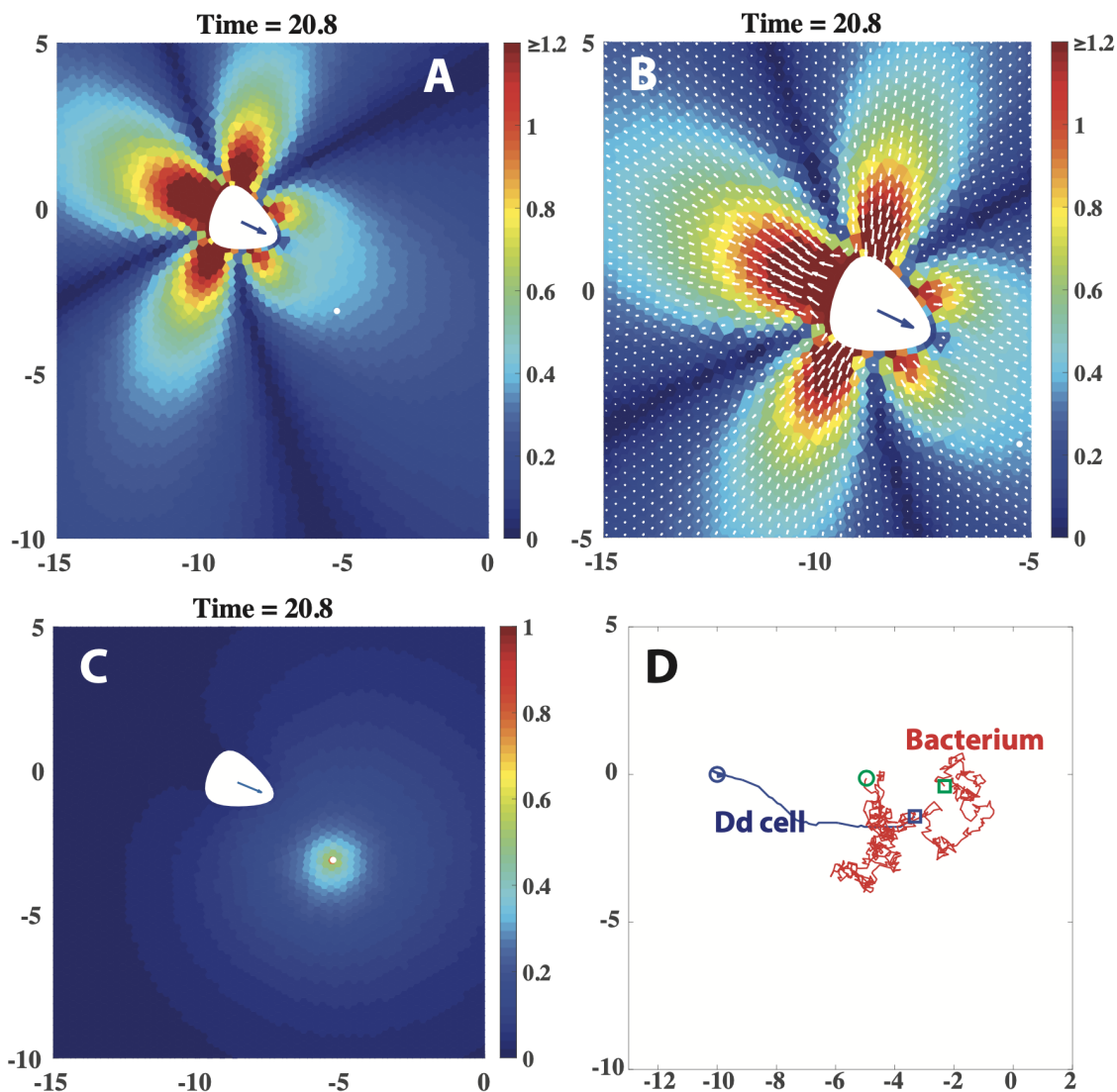


Figure 3: **Simulation of a swimming Dd cell following a bacterium guided by chemotaxis.** **AB** Snapshots of the fluid velocity at $T = 20.8$, where the heatmap (**B**) shows the amplitude of the fluid velocity, in the zoom in view near the Dd cell (**C**), the white arrows show the fluid velocity directions. **C** A snapshot of the heatmap of the diffusive folate signal concentration at $T = 20.8$. In **ABC**, both the Dd cell and the bacterium are colored in white. **D** trajectories of the Dd cell (blue) and the bacterium (red), where circles show the start points of the Dd cell center (blue circle) and the bacterium (green circle), and squares show the end points of the Dd cell center (blue square) and the bacterium (green square). The Dd cell catches the bacterium after 69 swimming cycles.

direction of the bacterium's jump ϑ is given by equation (2), and it takes the + sign if the bacterium prefers to move with the flow, and the - sign if against the flow.

We performed three groups of simulations: 1) no bacterial rheotaxis, 2) bacterial

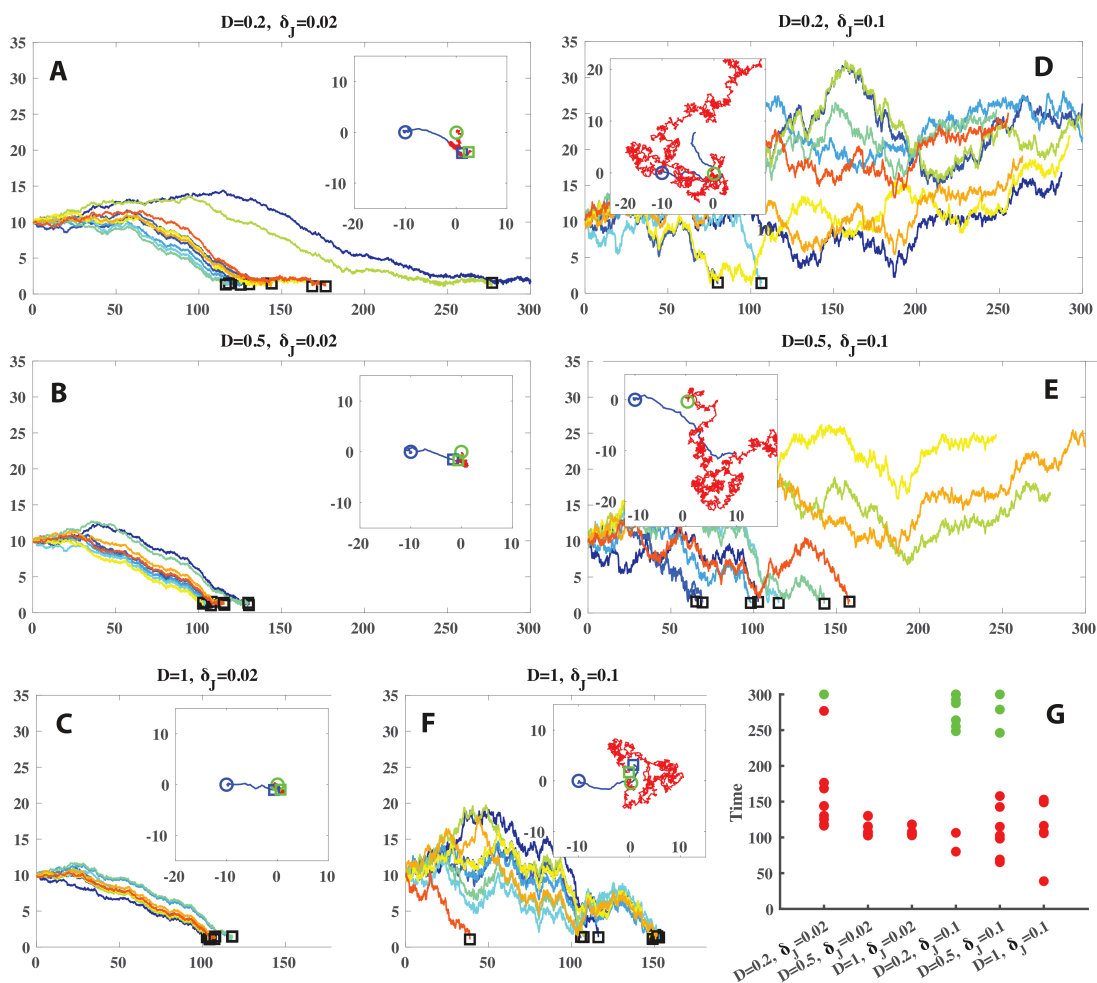


Figure 4: **Simulation results of chemotaxis guided Dd cell swimming.** **A-F** Distance between the Dd cell center and the bacterium with different combinations of D and δ_J values. x -axis shows the time counted as swimming cycles. Each colored curve shows the result from one simulation from the group, and black boxes show when the Dd cell catches the bacterium. The sub-panel in each panel shows the trajectories of the Dd cell (blue curve) and the bacterium (red curve) from one typical simulation from the group, with the blue and green circles mark the starting locations of the Dd cell and the bacterium, and the blue and green squares mark the end locations of the Dd cell and the bacterium when the Dd cell catches the bacterium. **G** Durations of the simulations, where red dots show when the Dd cell catches the bacterium, green dots show when the bacterium runs out of $\Omega_{\text{Chem}} : [-25, 25] \times [-25, 25]$, or the Dd cell does not catch the bacterium by the end of 300 cycles.

rheotaxis with a biased random walk with the flow, and 3) bacterial rheotaxis with a biased random walk against the flow. We take $D = 1$, $\delta_J = 0.05$ in all three groups, and in each group we run 10 simulations. Simulation results are shown in figure 5. Without bacterial rheotaxis, the Dd cell catches the bacterium in all 10 simulations (figure 5AD).

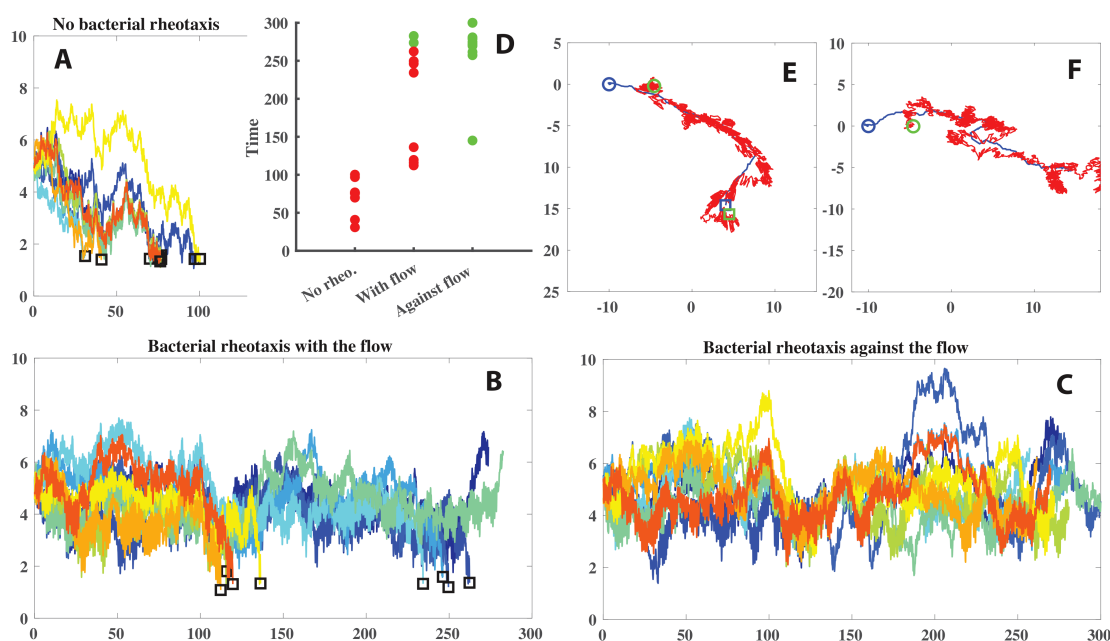


Figure 5: **Simulation results of bacterial rheotaxis.** **A** **B** **C** Distance between the bacterium and the Dd cell center with **A** no bacterial rheotaxis, **B** bacterial rheotaxis with the flow, and **C** bacterial rheotaxis against the flow. x -axis shows the time counted as swimming cycles. Each colored curve shows the result from one simulation from the group, and black boxes in **A** **B** **C** show when the Dd cell catches the bacterium. **D** Durations of the simulations, where red dots mark the time when the Dd cell catches the bacterium, green dots mark when the bacterium runs out of $\Omega_{\text{Chem}} : [-25, 25] \times [-25, 25]$, or the Dd cell does not catch the bacterium by the end of 300 cycles. **E** Trajectories of the Dd cell (blue curve) and the bacterium (red curve) with bacterial rheotaxis with the flow, with the blue and green circles mark the starting locations of the Dd cell and the bacterium, and the blue and green squares mark the end locations of the Dd cell and the bacterium when the Dd cell catches the bacterium. **F** Trajectories of the Dd cell (blue curve) and the bacterium (red curve) with bacterial rheotaxis against the flow, with the blue and green circles mark the starting locations of the Dd cell and the bacterium, the Dd cell does not catch the bacterium in 300 cycles.

With bacterial rheotaxis with the flow, in 8 out of 10 simulations it needs longer time for the Dd cell to catch the bacterium and 8 out of 10, and in the other 2 simulations the bacterium runs out of the Ω_{Chem} domain after > 250 Dd cell swimming cycles (figure 5BD). Finally with bacterial rheotaxis against the flow, in 8 out of 10 simulation the bacterium runs out of the Ω_{Chem} domain, and in the other 2 simulations the bacterium stays within the Ω_{Chem} domain always but the Dd cell does not catch the bacterium in 300 cycles (figure 5CD). Figure 5E shows the trajectories of the Dd cell and the bacterium with bacterial rheotaxis with the flow from one simulation, when the Dd cell catches the bacterium at the end, and figure 5F shows the trajectories of the Dd cell and the bacterium with bacterial rheotaxis against the flow from another simulation,

the Dd cell does not catch the bacterium in 300 cycles.

Our simulation results (figure 5) show that while bacterial rheotaxis against the flow appears to be a good strategy for the bacterium to escape from the predator Dd cell, bacterial rheotaxis with the flow may also help the bacterial to run away a little compared to no rheotaxis. We emphasize that at LRN, since inertia is absent, the current flow profile only depends on the current Dd cell deformation, and it keeps changing over a swimming cycle (see Figure F1). The bacterial rheotaxis we find here is the result out of one or even multiple Dd cell swimming cycles. Moreover, we would also point out that even in the best simulated scenario – bacterial rheotaxis against the flow, the bacterium is not able to fully escape from the Dd cell, which can be seen from figure 5C that the distance between the Dd cell and the bacterium oscillates but the mean is not increasing, indicating that the Dd cell keeps following the bacterium.

3.3. Chemotaxis guided amoeboid swimming caused by a dilute suspension of bacteria

Finally we consider the system with one Dd cell and a dilute suspension of bacteria, that is, a small number of bacteria present in the system. In the dilute suspension, the hydrodynamic interactions among the bacteria can be ignored. We consider systems where initially a group of N bacteria locate equispaced in a ring with the Dd cell center as the ring center (see supplement movie and Figures F6 - F8, the color scales are the same as figure 3C), and $D = 1$, $\delta_J = 0.1$ in all simulations in this section.

Simulations results show that similar to the systems with only one bacterium, when multiple bacteria are present, the Dd cell is still able to follow the chemoattractant signals and catch some bacteria. However, we notice that unlike in the systems with only one bacterium where the Dd cell movement is more directed, now with more bacteria present, the movement of the Dd cell becomes more chaotic – the Dd cell changes its polarization between consecutive cycles more frequently. To quantify this effect, we define a Dd cell polarized orientation change index PCI as follows:

$$\text{PCI}_n = \frac{1 - \cos(\theta_n - \theta_{n-1})}{2}, \quad n \geq 2, n \in \mathbb{N}$$

where PCI_n denotes the PCI for the n th swimming cycle $t \in [nT, (n+1)T)$, and θ_n is the Dd cell polarization angle in the n th cycle. PCI_n takes values in $[0, 1]$, with $\text{PCI}_n = 0$ means that the polarization does not change between the two consecutive cycles, while $\text{PCI}_n = 1$ means that the polarization changes with an angle π , i.e., the polarization is reversed.

We compare simulation results between systems with one bacterium only and systems with multi bacteria, the former group includes single bacterium with no external flow (figure 6AA'), single bacterium with rheotaxis along the flow (figure 6BB') and against the flow (figure 6CC'), and the latter multi bacteria group includes 6, 8 or 12 bacteria with no external flow (figure 6DD', EE', FF'). In the initial stage of all the simulations, the chemoattractant signal has not diffused to the whole Dd cell, causing a random polarization of the cell. Therefore, PCI is high in a small period at the beginning

stage. After the initial stage, the Dd cell is able to receive the diffusive chemoattractant signal. In the systems (no rheotaxis, rheotaxis along and against the flow) with only one bacterium, the averagely low PCI indicates that the Dd cell performs a more directed swimming toward the bacterium (figure 6ABC). On the other hand, PCI is averagely high when more bacteria are present, indicating that the polarization decision of the Dd cell is affected by many body effect, and thus presents a chaotic behavior without the ability to effectively follow and catch a bacterium. Looking further into the dynamics of the chemotaxis guided amoeboid swimming (supplement movie and Figures F6 - F8), we find that the number multiplication of bacteria plays a similar role as the period multiplication as a road transition to the chaos [60]. Due to the Dd cell surrounded by multiple strong signal sources, the polarization of the Dd cell is frequently changed. In each of simulations in 6, we track the R_f concentrations at four sites along the Dd cell boundary, with each neighboring pair separated by an angle of $\pi/2$, and the results are given in the bottom panels in figure 6A' - F'. With only one bacterium in the system (figure 6A'B'C'), R_f at the four sites are averagely low (mostly below 0.6), and it is clear that which site is at the front / rear, as its R_f keeps the highest / lowest all the time (purple / orange line in figure 6A'B'C'). Such a clear difference in the R_f level indicates a clear polarization of the Dd cell. On the other hand, when more bacteria are presented in the system, R_f levels are much higher (figure 6D'E'F'), and there is no clear high / low difference in the R_f at the four sites due to the high level as well as noise, leading to the frequent change in the cell polarization as is shown by the PCI plots. This causes the chaotic swimming pattern and reduces the cell's efficiency in catching bacteria. As pointed out above, this chaotic polarization behavior becomes more evident with more bacteria present in the system, which is verified by larger average PCIs in figure 6F compared to figure 6DE.

4. Discussion

While Dd amoeboid cell has long been well known as a model system for chemotaxis study on a crawling based motion, in recent year, Dd cell swimming induced by different types of taxis including chemotaxis has become an emerging research area. A major modeling challenge in this direction is the coupling of signaling dynamics and hydrodynamics. In this paper, we developed a minimal modeling framework to investigate the chemotaxis induced amoeboid cell swimming. Our model captures the interactions between a Dd cell and bacteria, where both biochemical (chemotaxis signaling dynamics) and biomechanical (amoeboid swimming and bacterial rheotaxis) are considered. For the numerical computations, a complex analysis technique - *mathematical amoeba model* [39, 45, 48–50] is applied to solve the amoeboid dynamics in 2D viscous flows, associated with the finite volume method based on the moving mesh Voronoi tessellation [55, 56] to solve the RDC equation system. Our simulations results show that chemotaxis effectively guides Dd cell swimming, especially when less bacteria are presented in the system, and bacterial rheotaxis may help a bacterium to escape

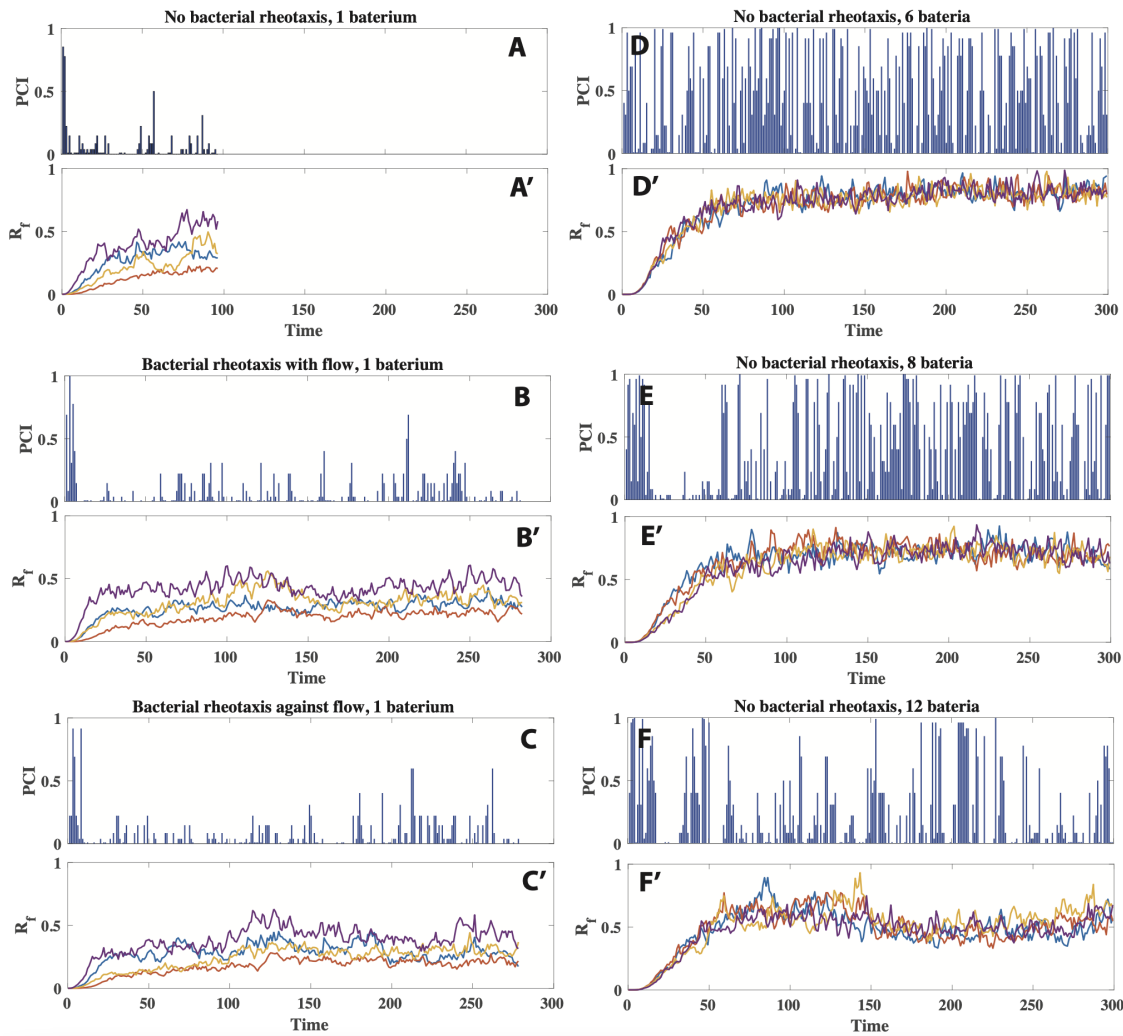


Figure 6: **Dd cell polarization change.** Each top panel (A - F) shows the PCI changes in one simulation with the conditions shown by the panel title, and the bottom panels (A' - F') shows the R_f concentration at four sites along the Dd cell boundary, with each neighboring pair separated by an angle of $\pi/2$. AA', BB', CC' show a more directed Dd cell swimming when guided by a single bacterium, whether with or without bacterial rheotaxis. DD', EE', FF' show a more chaotic Dd cell swimming when surrounded by more bacteria.

from a predator Dd cell.

To better investigate the dynamics of chemotaxis induced amoeboid cell swimming, there are many aspects that our model can be developed. We discuss some major aspects in the following.

Intracellular signaling dynamics induced amoeboid cell shape deformations. In this paper, we used the 2D *mathematical amoeba model* (section 2.3), which was greatly used in modeling study of amoeboid cell swimming. However, the shape deformations in the mathematical amoeba model is prescribed. In the future, we plan

to develop an intracellular submodel for the amoeboid cell to capture how the membrane protein dynamics in response to extracellular stimuli generates excitable traveling waves of cell shape deformations. Several modeling approaches to this directions have been developed, including models with a phenomenological description of membrane protein reaction-diffusion system that generates excitable dynamics of cell membrane deformation [46, 47] and a crawling based chemotaxis induced amoeboid cell deformation and migration model [61]. We would like to mention that the modeling framework developed in this paper is compatible with more complex cell deformations, using the computational method developed in [39].

Chemotaxis induced amoeboid swimming in confined space. Currently in our model, we consider a swimming system in free space. However, amoeboid motion generally occurs close to surfaces, in small capillaries or in extracellular matrices of biological tissues. In addition, micro-organisms swim through permeable boundaries, cell walls, or microvasculature. For example, flows are ubiquitous in human immune systems, blood vessels and microcirculation system, and are subjected to biological confinement by complex geometric structures. In particular, the effect of walls on motile micro-organisms has been a topic of increasingly active research. Recently, theoretical and modeling studies have revealed complicated swimming trajectories with the confinement effects and simulation predictions have been verified by experiments [40, 41, 62, 63]. In the future we will develop our model to study a swimming system in confined space.

Hydrodynamic interactions and chemotaxis of bacteria. In this paper we consider only a dilute suspension of bacteria, and we neglect bacterium - bacterium and bacterium - Dd cell hydrodynamic interactions. Due to the large size ratio of the Dd cell to a bacterium, the hydrodynamic effects generated by a bacterium should not affect much of the Dd cell swimming dynamics, yet the hydrodynamic interactions between bacteria might play an important role to bacterial swimming as well as the chemotaxis dynamics when the concentration of bacteria is higher. In recent years, both modeling and experimental studies reveal that in an active suspension of bacteria, hydrodynamics affects bacterial collective motions with chemotaxis [64, 66–69]. Another important future direction to our current modeling study would thus be to consider an active suspension of bacteria with hydrodynamic interactions.

In addition, it is well known that *E. coli* also respond to chemotactic signals, either produced by themselves or following local chemical gradients [65, 69, 70]. Yet whether bacterial chemotaxis play a role in the Dd - *E. coli* swimming system stays unclear. Would bacterial chemotaxis help *E. coli* to run away from the Dd cell is another interesting question to be considered and investigated, on both experimental and modeling sides. In particular, two crucial questions should be addressed: will the Dd send the signal to repel / attract the *E. coli*? With a large amount of *E. coli* presented in the system, how will the chemotaxis induced bacterial clustering alter the Dd - *E. coli* interaction?

Acknowledgments

The authors acknowledge partial support from the National Science Foundation Grant DMS-1951184 to QW. Simulations were performed using the computer clusters and data storage resources of the HPCC at University of California, Riverside, which were funded by grants from NSF (MRI-1429826) and NIH (1S10OD016290-01A1).

Appendix A. Goursat's formula and the conformal representation of the Dd cell

Consider the Dd cell swimming in an incompressible Newtonian fluid of density ρ , viscosity μ , and velocity \mathbf{u} , the fluid dynamics is governed by the Navier-Stokes equations:

$$\rho \frac{\partial \mathbf{u}}{\partial t} + \rho(\mathbf{u} \cdot \nabla)\mathbf{u} = -\nabla p + \mu \Delta \mathbf{u} + \mathbf{f} \quad (\text{A.1})$$

$$\nabla \cdot \mathbf{u} = 0 \quad (\text{A.2})$$

where the external force field \mathbf{f} should vanish in a swimming problem as the cell totally depends on self-propulsion. For the swimming Dd cell, let L, U, ω be the characteristic scales of length, speed and frequency of shape deformations, respectively. We introduce two dimensionless variables: Reynolds number $\text{Re} = \rho LU/\mu$ and the Strouhal number $\text{Sl} = \omega L/U$. The Navier-Stokes equations (A.1, A.2) can be converted into dimensionless form:

$$\text{Re} \cdot \text{Sl} \frac{\partial \mathbf{u}}{\partial t} + \text{Re}(\mathbf{u} \cdot \nabla)\mathbf{u} = -\nabla p + \Delta \mathbf{u} \quad (\text{A.3})$$

$$\nabla \cdot \mathbf{u} = 0 \quad (\text{A.4})$$

The small size (L) and low speed (U) of cells leads to $\text{Re} \ll 1$, and in this low Reynolds number flow regime cells move by exploiting the viscous resistance of the fluid. Dd cells have a typical length of $L \sim 25 \mu\text{m}$, swim at $U \sim 3 \mu\text{m}/\text{min}$ and a period of shape deformation cycle $T \sim 1 - 2 \text{min}$ that gives the deformation frequency $\omega \sim 1 \text{min}^{-1}$ [36, 37]. Assume the medium is water ($\rho \sim 10^3 \text{kg} \cdot \text{m}^{-3}$, $\mu \sim 10^{-3} \text{Pa} \cdot \text{s}$), thus $\text{Re} \sim O(10^{-6})$ and $\text{Sl} \sim O(10^{-4})$. For such a system, both inertial terms on the left hand side of equation (A.3) can be neglected, and the flow is governed by the Stokes equations:

$$\Delta \mathbf{u} - \nabla p = \mathbf{0}, \quad \nabla \cdot \mathbf{u} = 0 \quad (\text{A.5})$$

In 2D the incompressibility condition $\nabla \cdot \mathbf{u} = 0$ in equation (A.5) can be satisfied by introducing a stream function $\Lambda(z, \bar{z}; t)$, which is a real-valued scalar potential such that $u = \partial_y \Lambda - i \partial_x \Lambda$, where $u \in \mathbb{C}$ is the complex representation of the velocity field \mathbf{u} , i.e., for $\mathbf{u} = (u_1, u_2)$, $u = u_1 + i u_2$. Then the Stokes equations (A.5) imply that Λ satisfies the biharmonic equation $\Delta^2 \Lambda = 0$, whose general solution can be expressed by Goursat's formula [59]

$$\Lambda(z, \bar{z}; t) = \Re[\bar{z}\phi(z; t) + \chi(z; t)]$$

where $\Re(\cdot)$ denotes the real part of the complex quantity; for any t , $\phi(z; t)$ and $\chi(z; t)$ are analytic functions in the infinite fluid domain $\Omega(t)_{\text{Cell}}^{\text{C}}$, known as the *Goursat functions*. Let $V(z, \bar{z}; t)$ be the velocity boundary condition determined by the cell's shape deformations, with $z \in \partial\Omega_{\text{Cell}}(t)$, and we assume no-slip boundary condition along the cell's boundary, then the 2D low Reynolds number swimming problem can be reduced to [49, 59]: find analytic functions $\phi(z; t)$ and $\psi(z; t) = \chi'(z; t)$ in the fluid domain, such that

$$\phi(z; t) - z\overline{\phi'(z; t)} - \overline{\psi(z; t)} = V(z, \bar{z}; t) \quad (z \in \partial\Omega_{\text{Cell}}(t)) \quad (\text{A.6})$$

Equation (A.6) will be referred to as the boundary condition constraint on the unknowns ϕ and ψ .

At time t , the Dd cell captures a simply connected bounded region $\Omega_{\text{Cell}}(t)$ in the complex z -plane using complex representation. Let $D = \{\zeta \in \mathbb{C} : |\zeta| < 1\}$ be the unit disk in the computational complex ζ -plane. The *Riemann mapping theorem* ensures the existence of a single-valued analytic conformal mapping $z = w(\zeta; t)$ which maps $\overline{\mathbb{C}/D}$ one-to-one and onto $\overline{\mathbb{C}/\Omega_{\text{Cell}}(t)}$ – the infinite fluid domain (Fig. A1), and preserves the correspondence of infinity, i.e., $w(\infty; t) = \infty$. Therefore the shapes of the Dd cell when observed from the reference frame can be described by the t -family of conformal mapping $\{z = w(\zeta; t)\}$. In addition, $z = w(\zeta; t)$ always has its Laurent expansion of the form [39]:

$$z = w(\zeta; t) = \alpha_1(t)\zeta + \alpha_0(t) + \frac{\alpha_{-1}(t)}{\zeta} + \frac{\alpha_{-2}(t)}{\zeta^2} + \cdots + \frac{\alpha_{-n}(t)}{\zeta^n} + \cdots (\text{A.7})$$

where $\alpha_1(t) \neq 0$ and $|\zeta| > 1$. The α_0 term gives the current location of the cell center, and the polarization can be indicated by the α_1 term. The Dd amoeboid cell boundary is thus given by

$$\partial\Omega_{\text{Cell}}(t) = \{z(t) = w(\sigma; t) | \sigma \in S^1\}$$

and the no-slip boundary condition can be written as

$$u(w(\sigma))(t) = \frac{\partial}{\partial t} w(\sigma; t)$$

Let $\phi(z, t)$ and $\psi(z, t)$ be the solutions to the boundary condition constraint given by equation (A.6), and let

$$\Phi(\zeta; t) = \phi(w(\zeta; t); t), \quad \Psi(\zeta; t) = \psi(w(\zeta; t); t) \quad (|\zeta| \geq 1)$$

thus $\Phi(\zeta; t)$ and $\Psi(\zeta; t)$ are functions on the ζ -plane which are analytic on \mathbb{C}/\overline{D} and continuous on \mathbb{C}/D at any time t . With the conformal mapping representation, equation (A.6) can be pulled back to the ζ -plane as a function on the unit disk S^1 :

$$\Phi(\sigma) - \frac{w(\sigma)}{w'(\sigma)} \overline{\Phi'(\sigma)} - \overline{\Psi(\sigma)} = V(\sigma) \quad (\sigma \in S^1) \quad (\text{A.8})$$

In general, the ζ^{-n} term with $n > 0$ in the conformal mapping equation (A.7) gives $n + 1$ angles along a round periphery of the swimmer. To approximate a real swimming Dd cell shape, we can first approximate the cell boundary by a N -polygon,

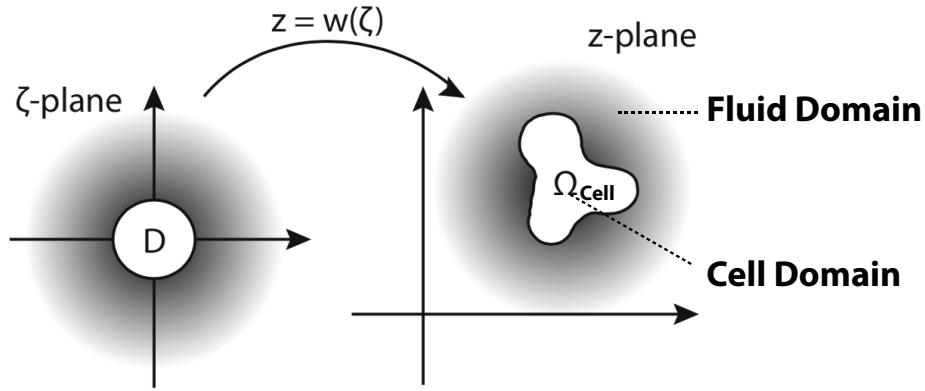


Figure A1: The conformal mapping $z = w(\zeta)$ from $\overline{\mathbb{C}/D}$ to $\overline{\mathbb{C}/\Omega_{\text{Cell}}}$, with Ω_{Cell} and $\overline{\mathbb{C}/\Omega_{\text{Cell}}}$ in the z -plane give the cell and fluid domains, respectively. Figure is reproduced from [39].

then obtain the corresponding conformal mapping using the Schwarz-Christoffel formula then truncate its Laurent expansion leaving a finite number of terms, from which we can solve equation (A.8) using the computational Muskhelishvili's method, as prescribed in [39].

Here we adopt a simple form of this mathematical amoeba model, where the shape of cell is in the form of

$$w(\zeta; t) = e^{i\theta(t)} \left[r(t)\zeta + \frac{\eta_{-1}(t)}{\zeta} + \frac{\eta_{-2}(t)}{\zeta^2} \right] + Z_{\text{Dd}}(t) \quad (\text{A.9})$$

where

- $r(t) \in \mathbb{R}$ controls the cell size. When the cell is at rest and in a circular shape ($\eta_{-1} = \eta_{-2} = 0$), r gives the cell radius, which we denote by r_0 . We assume that as the cell swims, there is no material exchange between the cell and the surrounding fluid, which validates the no-slip boundary condition. In 2D it naturally becomes the area conservation constraint, described by the following equation:

$$\text{Area}(t) = \frac{1}{2} \Im \oint \bar{w} dw \equiv \pi r_0^2$$

where \Im denotes the imaginary part of the complex quantity. With w given by equation (A.9), the area conservation constraint can be reduced to:

$$\begin{aligned} \text{Area}(t) &= \pi \left(r^2(t) - |\eta_{-1}(t)|^2 - 2|\eta_{-2}(t)|^2 \right) \equiv \pi r_0^2 \\ \Rightarrow \quad r(t) &= \sqrt{r_0^2 + |\eta_{-1}(t)|^2 + 2|\eta_{-2}(t)|^2} \end{aligned} \quad (\text{A.10})$$

- $\theta(t) \in \mathbb{R}$ gives the cell polarization that will be determined by signaling sensing dynamics as discussed in the Section Appendix B. In particular, we assume that the polarization θ is determined at the beginning of a swimming cycle and will not change during the cycle, thus $\theta(nT + t) \equiv \theta(nT)$ during the n th swimming cycle with $t \in [0, T)$.

- $\eta_{-1}(t), \eta_{-2}(t) \in \mathbb{R}$ give the shape deformations. They are real-valued functions so that the cell swims in a straight line once the polarization θ is determined from signaling dynamics.
- $Z_{\text{Dd}}(t)$ gives the location of the cell, while $U_{\text{Dd}}(t) = \dot{Z}_{\text{Dd}}(t)$ gives the velocity of the cell which is computed through cell-fluid interaction discussed as follows.

In the case that the conformal mapping equation (A.7) includes only the ζ^{-1}, ζ^{-2} in the negative order terms in its Laurent expansion, the solution to equation (A.8) is given by [49, 50]:

$$\begin{aligned}\Phi(\zeta) &= \dot{Z}_{\text{Dd}} + \frac{\dot{\alpha}_{-1}}{\zeta} + \frac{\dot{\alpha}_{-2}}{\zeta^2} \\ \Psi(\zeta) &= -\frac{\bar{\alpha}_1}{\zeta} + \frac{\bar{\alpha}_{-2} + \frac{\bar{\alpha}_{-1}}{\zeta} + \frac{\bar{\alpha}_1}{\zeta^3}}{\alpha_1 - \frac{\alpha_{-1}}{\zeta^2} - \frac{2\alpha_{-2}}{\zeta^3}} \left(\dot{\alpha}_{-1} + \frac{2\dot{\alpha}_{-2}}{\zeta} \right)\end{aligned}$$

In particular, with w given by equation (A.9) and that $\theta(nT + t) \equiv \theta(nT)$ during each swimming stroke, we have

$$\Phi(\zeta) = e^{i\theta} \left(\frac{\eta_{-2}\dot{\eta}_{-1}}{r} + \frac{\dot{\eta}_{-1}}{\zeta} + \frac{\dot{\eta}_{-2}}{\zeta^2} \right) \quad (\text{A.11})$$

$$\Psi(\zeta) = e^{-i\theta} \left[-\frac{\dot{r}}{\zeta} + \frac{\eta_{-2} + \frac{\eta_{-1}}{\zeta} + \frac{r}{\zeta^3}}{r - \frac{\eta_{-1}}{\zeta^2} - \frac{2\eta_{-2}}{\zeta^3}} \left(\dot{\eta}_{-1} + \frac{2\dot{\eta}_{-2}}{\zeta} \right) \right] \quad (\text{A.12})$$

where

$$\begin{aligned}U_{\text{Dd}} &= \dot{Z}_{\text{Dd}} = e^{i\theta} \frac{\eta_{-2}\dot{\eta}_{-1}}{r} \\ \dot{r} &= \frac{\eta_{-1}\dot{\eta}_{-1} + 2\eta_{-2}\dot{\eta}_{-2}}{\sqrt{r_0^2 + \eta_{-1}^2 + 2\eta_{-2}^2}}\end{aligned} \quad (\text{A.13})$$

The velocity field of the surrounding flow is thus given by the formula

$$u(\zeta, \bar{\zeta}) = \Phi(\zeta) - \frac{w(\zeta)}{w'(\zeta)} \overline{\Phi'(\zeta)} - \overline{\Psi(\zeta)} \quad (|\zeta| \geq 1) \quad (\text{A.14})$$

$u(\zeta, \bar{\zeta})$ induces the velocity function u_z on the z -plane:

$$u_z(z) = u(\zeta = w^{-1}(z))$$

With $z = w(\zeta)$ given by equation (A.9), by Lagrange inversion formula, we have

$$\frac{1}{\zeta} = \frac{e^{i\theta} r}{z - Z_{\text{Dd}}} + \frac{e^{3i\theta} r^2 \eta_{-1}}{(z - Z_{\text{Dd}})^3} + \frac{e^{4i\theta} r^3 \eta_{-2}}{(z - Z_{\text{Dd}})^4} + O\left(\frac{1}{(z - Z_{\text{Dd}})^5}\right) \quad (\text{A.15})$$

We use equation (A.15) to obtain an approximate for $u_z(z)$:

$$u_z(z) = u(\zeta = w^{-1}(z)) \sim u\left(\left(\frac{e^{i\theta} r}{z - Z_{\text{Dd}}} + \frac{e^{3i\theta} r^2 \eta_{-1}}{(z - Z_{\text{Dd}})^3} + \frac{e^{4i\theta} r^3 \eta_{-2}}{(z - Z_{\text{Dd}})^4}\right)^{-1}\right) \quad (\text{A.16})$$

In the following discussion for simplicity we use $u(z)$ to denote $u_z(z)$.

Appendix B. Signaling induced Dd cell polarization and shape deformations

We assume that the Dd cell undergoes shape deformations in response to signal gradient, with each swimming stroke lasting for a period of $[0, T]$ and consisting of three phases: (I) *polarization*, (II) *swimming*, (III) *relaxation*.

- (i) *Polarization*. At the beginning of each cycle, the amoeba is of a circular shape with no polarization, i.e., $w(\zeta) = r_0\zeta + Z_{\text{Dd}}$. The R_f concentration is numerically evaluated at each \mathbf{w}'_j . If

$$\max_{1 \leq j \leq N_r} \{R_f(\mathbf{w}'_j)\} - \min_{1 \leq j \leq N_r} \{R_f(\mathbf{w}'_j)\} < \varepsilon_R$$

for some threshold $\varepsilon_R > 0$, we randomly choose a polarization direction θ_T . Otherwise, we find the node \mathbf{w}'_K that has the maximum R_f value: $R_f(\mathbf{w}'_K) = \max_{1 \leq j \leq N_r} \{R_f(\mathbf{w}'_j)\}$. Then θ_K corresponding to \mathbf{w}'_K defines the polarization of the following stroke:

$$\theta_T = \theta(t)|_{t \in [0, T]} \equiv \theta_K = -i \ln \left(w^{-1}(\mathbf{w}'_K) \right)$$

Once the polarization θ_T is determined, in a short period $[0, T_P] \subset [0, T]$, the Dd cell stretches itself from a circular shape to an ellipse with its semi-major axis lying along the θ_T direction:

$$w(\zeta; t) = e^{i\theta_T} \left[r(t)\zeta + \frac{\eta_{-1}(t)}{\zeta} \right] + Z_{\text{Dd}}(t), \quad t \in [0, T_P] \quad (\text{B.1})$$

where we can choose $\eta_{-1}(t)$ to be the following linear function:

$$\eta_{-1}(t) = \frac{t}{T_P} \bar{\eta}, \quad t \in [0, T_P]$$

such that $\eta_{-1}(0) = 0$ gives the circular shape, and $\eta_{-1}(T_P) = \bar{\eta}$ gives an ellipse with semi-major and semi-minor axis lengths $r(T_P) + \bar{\eta}$ and $r(T_P) - \bar{\eta}$, respectively. The deformation in this stage will not result in net translation according to the *scallop theorem* [?], thus $Z_{\text{Dd}}(t) \equiv Z_{\text{Dd}}(0)$ for $t \in [0, T_P]$.

- (ii) *Swimming*. After polarized, the Dd cell undergoes the following shape deformations in a time interval $[T_P, T_P + T_S] \subset [0, T]$ which leads to active swimming along the polarization direction as is discussed in Section Appendix A:

$$w(\zeta; t) = e^{i\theta_T} \left[r(t)\zeta + \frac{\bar{\eta} \cos(2\pi\tau)}{\zeta} - \frac{\bar{\eta} \sin(2\pi\tau)}{\zeta^2} \right] + Z_{\text{Dd}}(t) \quad (\text{B.2})$$

where $\tau = (t - T_P)/T_S$.

- (iii) *Relaxation*. After the amoeboid cell returns to the ellipse shape at $t = T_P + T_S$, in the followed $[T_P + T_S, 2T_P + T_S] \subset [0, T]$ period the Dd cell undergoes the reversed shape deformations as defined in equation (B.1) but with

$$\eta_{-1}(t) = \frac{T - t}{T_P} \bar{\eta}, \quad t \in [T_P + T_S, T]$$

where T_P, T_S should satisfy $2T_P + T_S = T$. The Dd cell returns to the initial circular shape by the end of the stroke $t = T$. Again, the deformation in this stage do not result in net translation, i.e., $Z_{\text{Dd}}(t) \equiv Z_{\text{Dd}}(T_P + T_S)$ for $t \in [T_P + T_S, T]$. A full swimming stroke is thus completed.

Appendix C. Nondimensionalization of the system

We nondimensionalize the system, with T (the duration of a Dd cell swimming cycle) and r_0 (the Dd cell radius when the cell is at rest) the characteristic spatial and temporal scales, and R_{\max} the characteristic length concentration scale:

$$t^* = \frac{t}{T}, \quad \mathbf{x}^* = \frac{\mathbf{x}}{r_0}, \quad z^* = \frac{z}{r_0}, \quad f^* = \frac{f}{R_{\max}/r_0},$$

$$R_f^{0,*} = \frac{R_f^0}{R_{\max}}, \quad R_f^* = \frac{R_f}{R_{\max}}, \quad dW^* = \frac{dW}{\sqrt{T}}$$

When substitute into the model equations, bacteria motion equation (Eq (1) in the main text) becomes:

$$d\mathbf{x}_n^* = \mathbf{u}^* dt^* + d\mathbf{X}_n^* \quad (\text{C.1})$$

The RDC equations (Eqs (3-5) in the main text) become:

$$\frac{\partial f^*}{\partial t^*} = D^* \Delta^* f^* - \mathbf{u}^* \cdot \nabla^* f^* + a^* \int \sum_{n=1}^{N_B} \delta(\mathbf{x}^* - \mathbf{x}_n^*) d\mathbf{x}^* \quad (\text{C.2})$$

$$D^* \mathbf{n} \cdot \nabla^* f^* = -k_+^* f^* R_f^{0,*} + k_-^* R_f^* \quad (\text{C.3})$$

$$\frac{\partial R_f^*}{\partial t^*} = k_+^* f^* R_f^{0,*} - k_-^* R_f^* - \gamma^* R_f^* + \varsigma^* R_f^* \frac{dW^*}{dt^*} \quad (\text{C.4})$$

where

$$\Delta^* = r_0^2 \Delta, \quad \nabla^* = r_0 \nabla, \quad D^* = \frac{DT}{r_0^2}, \quad k_+^* = \frac{k_+ R_{\max} T}{r_0}, \quad k_-^* = k_- T,$$

$$a^* = \frac{a r_0 T}{R_{\max}}, \quad \gamma^* = \gamma T, \quad \varsigma^* = \varsigma \sqrt{T}$$

The cell shape equation (A.9) and the area conservation constraint equation (A.10) become

$$w^* = e^{i\theta} \left[r^* \zeta + \frac{\eta_{-1}^*}{\zeta} + \frac{\eta_{-2}^*}{\zeta^2} \right] + Z_{\text{Dd}}^* \quad (\text{C.5})$$

$$r^* = \sqrt{1 + |\eta_{-1}^*|^2 + 2|\eta_{-2}^*|^2} \quad (\text{C.6})$$

with

$$r^*(t^*) = \frac{r(t^*)}{r_0}, \quad \eta_{-1}^*(t^*) = \frac{\eta_{-1}(t^*)}{r_0}, \quad \eta_{-2}^*(t^*) = \frac{\eta_{-2}(t^*)}{r_0}$$

$$U_{\text{Dd}}^* = \frac{dZ_{\text{Dd}}^*}{dt^*} = e^{i\theta} \frac{\eta_{-2}^*}{r^*} \frac{d\eta_{-1}^*}{dt^*}$$

The fluid velocity field equation (A.14) becomes:

$$u^*(\zeta, \bar{\zeta}) = \Phi^*(\zeta) - \frac{w^*(\zeta)}{w^{*'}(\zeta)} \overline{\Phi^{*'}(\zeta)} - \overline{\Psi^*(\zeta)} \quad (|\zeta| \geq 1) \quad (\text{C.7})$$

where the non-dimensional Goursat's functions are:

$$\Phi^* = \frac{T}{r_0} \Phi, \quad \Psi^* = \frac{T}{r_0} \Psi$$

The inverse of the conformal mapping equation (A.15) becomes

$$\frac{1}{\zeta} = \frac{e^{i\theta} r^*}{z^* - Z_{\text{Dd}}^*} + \frac{e^{3i\theta} r^{*2} \eta_{-1}^*}{(z^* - Z_{\text{Dd}}^*)^3} + \frac{e^{4i\theta} r^{*3} \eta_{-2}^*}{(z^* - Z_{\text{Dd}}^*)^4} + O\left(\frac{1}{(z^* - Z_{\text{Dd}}^*)^5}\right) \quad (\text{C.8})$$

From equations (A.11, A.12) we have

$$\Phi^*(\zeta) = e^{i\theta} \left(\frac{\eta_{-2}^*}{r^*} \frac{d\eta_{-1}^*}{dt^*} + \frac{1}{\zeta} \frac{d\eta_{-1}^*}{dt^*} + \frac{1}{\zeta^2} \frac{d\eta_{-2}^*}{dt^*} \right) \quad (\text{C.9})$$

$$\Psi^*(\zeta) = e^{-i\theta} \left[-\frac{1}{\zeta} \frac{dr^*}{dt^*} + \frac{\eta_{-2}^* + \frac{\eta_{-1}^*}{\zeta} + \frac{r^*}{\zeta^3}}{r^* - \frac{\eta_{-1}^*}{\zeta^2} - \frac{2\eta_{-2}^*}{\zeta^3}} \left(\frac{d\eta_{-1}^*}{dt^*} + \frac{2}{\zeta} \frac{d\eta_{-2}^*}{dt^*} \right) \right] \quad (\text{C.10})$$

where from equation (A.13)

$$\frac{dr^*}{dt^*} = \frac{1}{\sqrt{1 + |\eta_{-1}^*|^2 + 2|\eta_{-2}^*|^2}} \left(\eta_{-1}^* \frac{d\eta_{-1}^*}{dt^*} + \eta_{-2}^* \frac{d\eta_{-2}^*}{dt^*} \right)$$

Finally we also give the expressions of w^* and Φ^* that will be used in calculating the fluid velocity field equation (C.7):

$$\begin{aligned} \frac{dw^*}{d\zeta} &= e^{i\theta} \left(r^* - \frac{\eta_{-1}^*}{\zeta^2} - \frac{2\eta_{-2}^*}{\zeta^3} \right) \\ \frac{d\Phi^*}{d\zeta} &= -e^{i\theta} \left(\frac{1}{\zeta^2} \frac{d\eta_{-1}^*}{dt^*} + \frac{2}{\zeta^3} \frac{d\eta_{-2}^*}{dt^*} \right) \end{aligned}$$

Appendix D. Local re-mesh of the fluid nodes near the Dd cell

To avoid clustering of fluid nodes near the cell boundary due to the Dd cell's large deformations, we apply two types of local re-mesh of the fluid nodes $\{\mathbf{w}_i\}$. First, at each time step, the closest layer of fluid nodes to the Dd cell is generated from the current conformal mapping w (equation (C.5), we omit the $*$ sign for dimensional quantities for simplicity and also in the following discussions) by taking equally spaced nodes along the contour generated by

$$w = e^{i\theta} \left[(1 + \epsilon)\sigma + \frac{\eta_{-1}}{\sigma} + \frac{\eta_{-2}}{\sigma^2} + Z_{\text{Dd}} \right], \quad \sigma \in S^1$$

for a small number $\epsilon \approx 0.3$. In addition, at the beginning of every cycle ($t = nT$), we re-generate fluid nodes in a local region near the cell boundary $\{\mathbf{x} \mid \|\mathbf{x} - \mathbf{x}_{\text{Dd}}\| < 3\}$ in a cubic lattice – the same as we initially generate the fluid mesh at $t = 0$, where \mathbf{x}_{Dd} is the Dd cell center position, and the distance is after nondimensionalization, i.e., the Dd cell has radius= 1 at rest. After each re-mesh, the f values at each newly generated node is taken to be the average of the three closest neighboring nodes from the old mesh. Finally we remove the old nodes in the re-meshed region.

Appendix E. Parameters

The parameter values used in our simulations are listed in the table below. Default values are for dimensionless quantities.

Parameters	Unit	Non-dimensionalization	Default Value
Bacterial motions			
δ_J	m	$\delta_J^* = \delta_J/r_0$	0.05
M	m/s	$M^* = TM/r_0$	1
Chemotaxis signaling dynamics			
D	m^2/s	$D^* = DT/r_0^2$	1
a	$\text{mol}/\text{m}^2\text{s}$	$a^* = ar_0T/R_{\max}$	1
k_+	$\text{m}^2/\text{mol}\cdot\text{s}$	$k_+^* = k_+R_{\max}T/r_0$	1
k_-	1/s	$k_-^* = k_-T$	0
γ	1/s	$\gamma^* = \gamma T$	0.2
ς	$1/\sqrt{\text{s}}$	$\varsigma^* = \varsigma\sqrt{T}$	0.1

Table E1: Parameter values.

The characteristic scales we used to non-dimensionalize the system are:

- T - the duration of a Dd cell swimming cycle;
- r_0 - the Dd cell radius when the cell is at rest;
- R_{\max} - characteristic length concentration of R_f .

From [36,37], we have an estimate of T about 1 – 1.5 minute; while for the cell size, only the length and width of a slender cell are available: $\sim 25\mu\text{m}$ long and $\sim 6\mu\text{m}$ wide as reported in [36], and $\sim 22\mu\text{m}$ long and $\sim 4\mu\text{m}$ wide as reported in [37], from which we can estimate that r_0 should be at the scale of $O(10)\mu\text{m}$. We are not aware of available data on R_{\max} .

If T , r_0 and R_{\max} can be measured in lab, estimates of all quantities in the system can be obtained from Table E1. For example, in our simulations we take $D^* \in [0.2, 1]$, $\delta_J^* \in [0.02, 0.1]$, with an estimate of $T = 1 \text{ min} = 60 \text{ s}$, $r_0 \sim 10\mu\text{m} = 10^{-5} \text{ m}$, then we estimate the range of D and δ_J should be about:

$$D \sim O(10^{-13} - 10^{-12}) \text{ m}^2/\text{s}, \quad \delta_J \sim O(10^{-7} - 10^{-6}) \text{ m}$$

Appendix F. Supplement figures

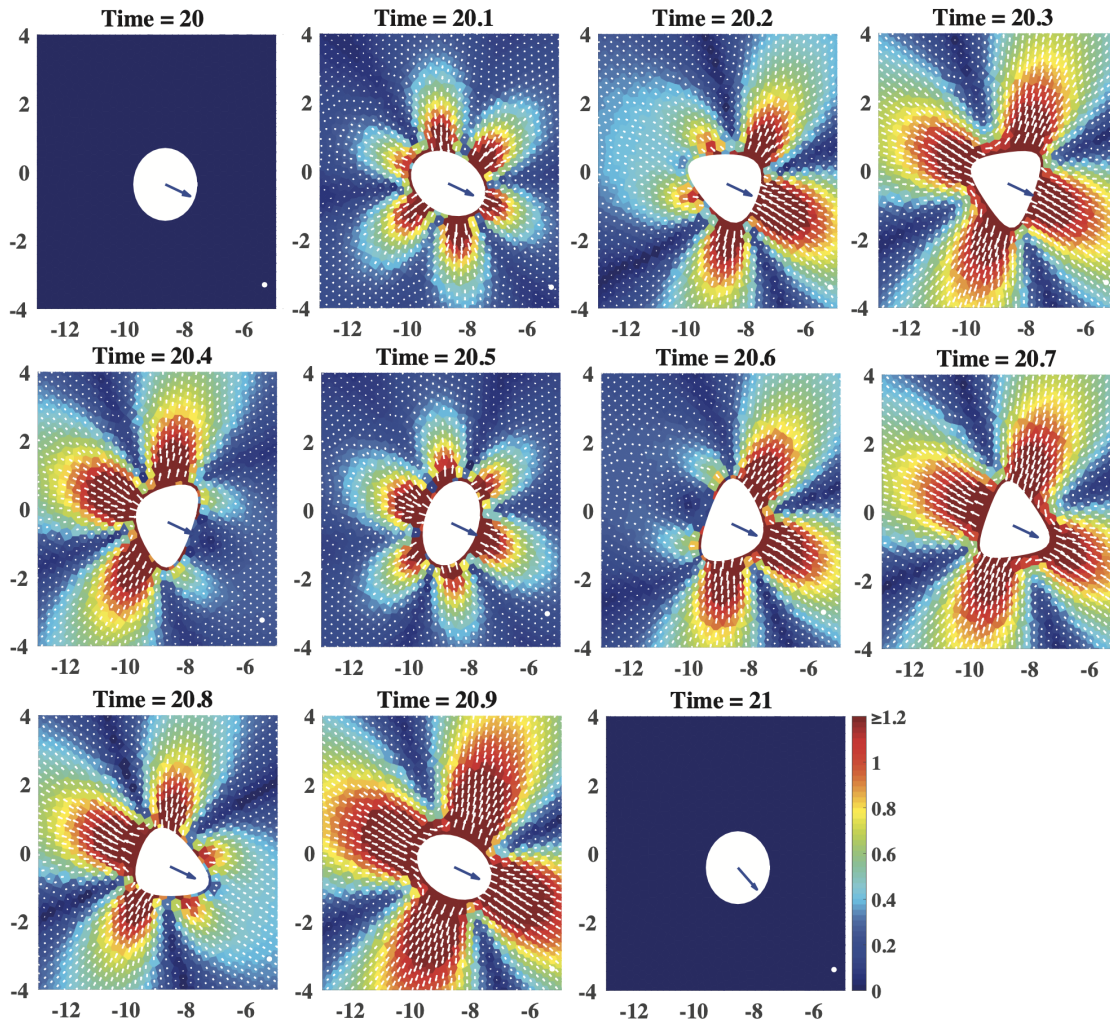


Figure F1: Time lapse snapshots of the fluid velocity profile during one Dd cell swimming cycle, where the heatmap shows the amplitude of the fluid velocity, and the white arrows show the fluid velocity directions. Notice that the flow directions keep changing with the cell deformation. For example, the flow is toward the cell from the back at Time=20.4, while at Time=20.7, the flow is away from the cell from the back.

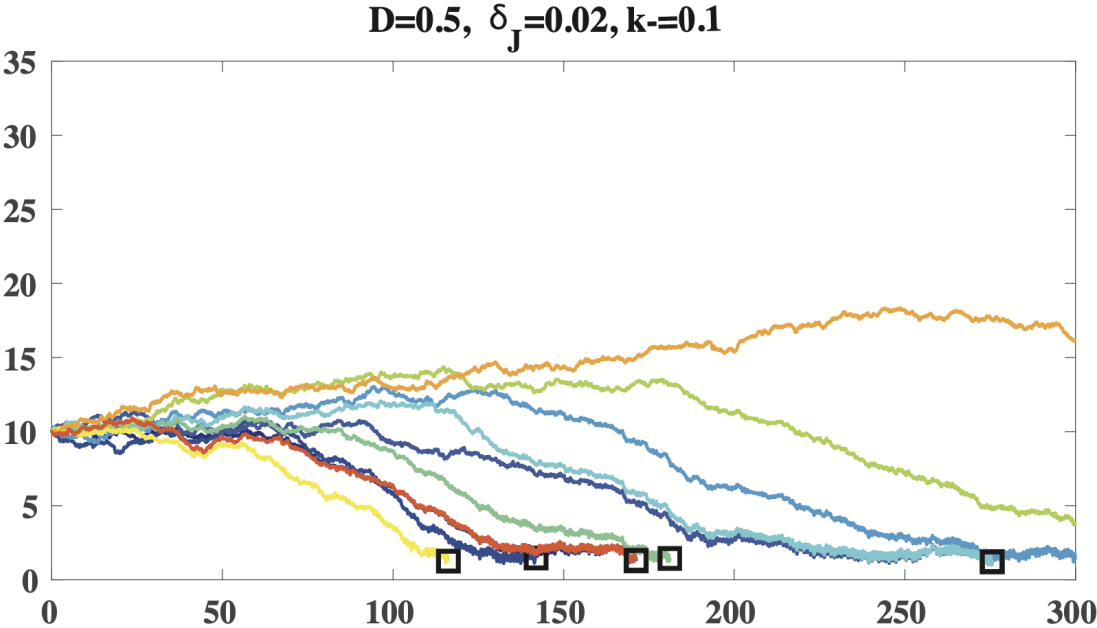


Figure F2: Distance between the Dd cell center and the bacterium with $D = 0.5$, $\delta_J = 0.02$ and $k_- = 0.1$. No bacterial rheotaxis.

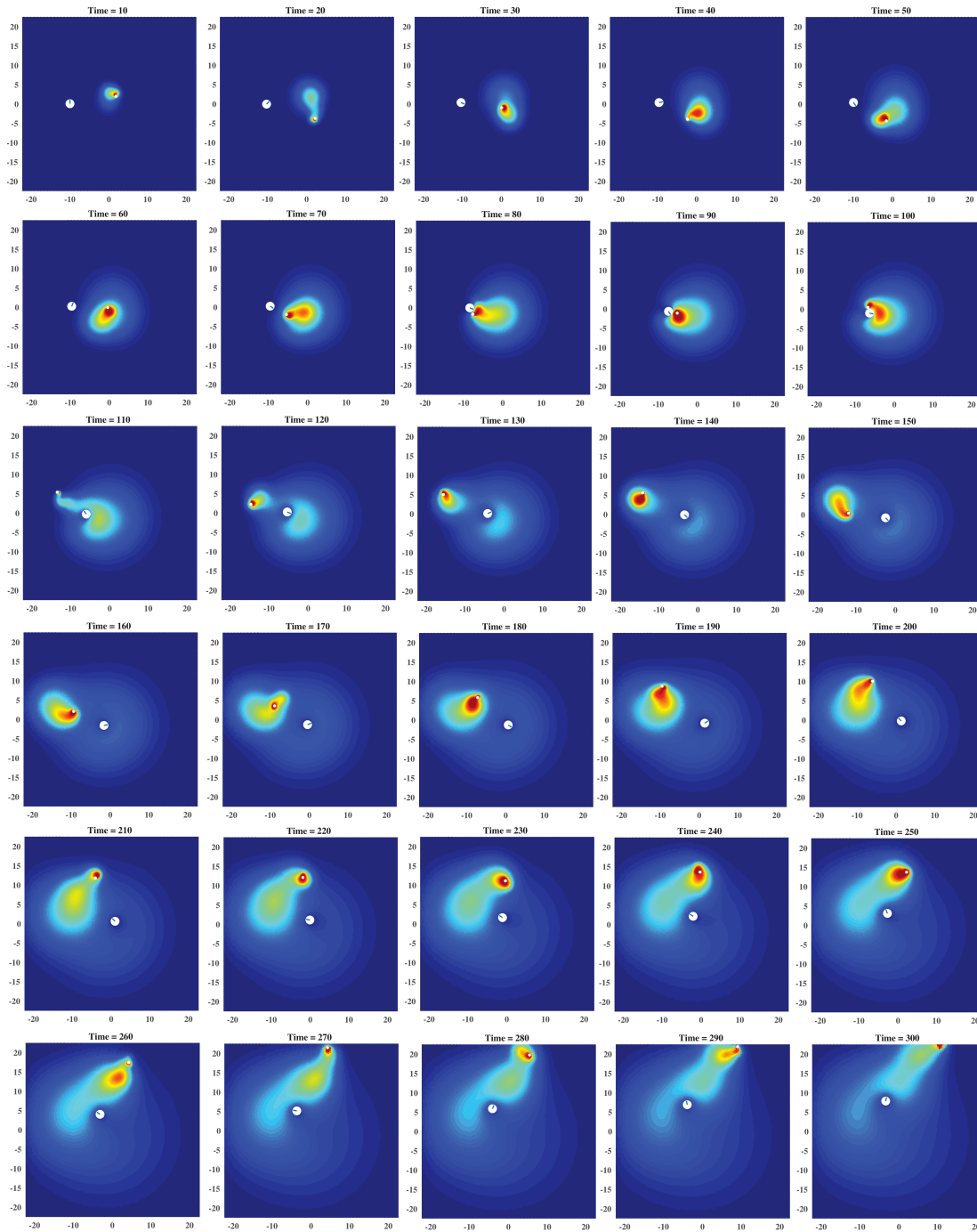


Figure F3: Time lapse snapshots of a typical simulation with $D = 0.2$, $\delta_J = 0.1$ and no bacterial rheotaxis. The color scale is the same as main figure 3C.

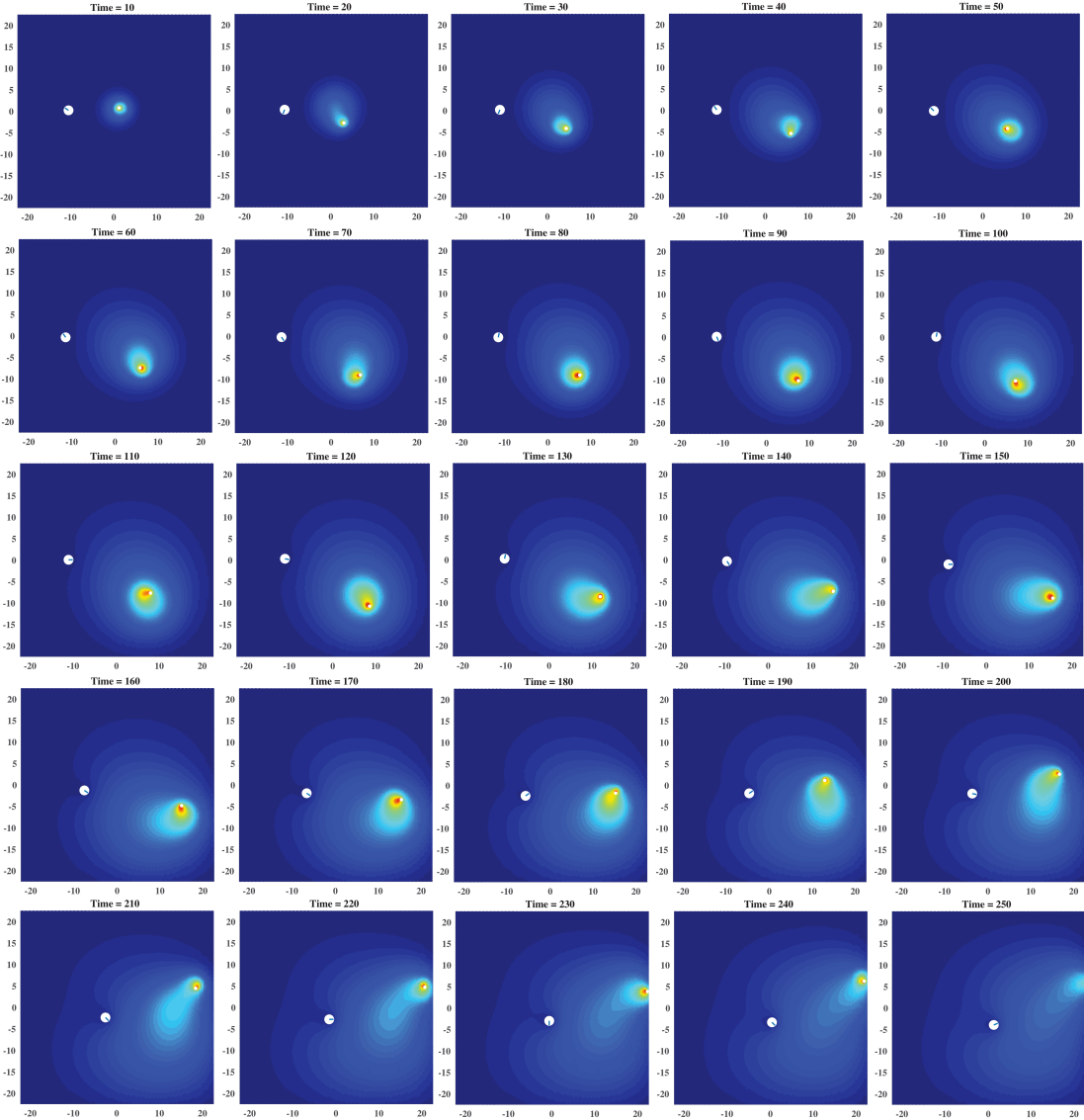


Figure F4: Time lapse snapshots of a typical simulation with $D = 0.5$, $\delta_J = 0.1$ and no bacterial rheotaxis. The color scale is the same as main figure 3C.

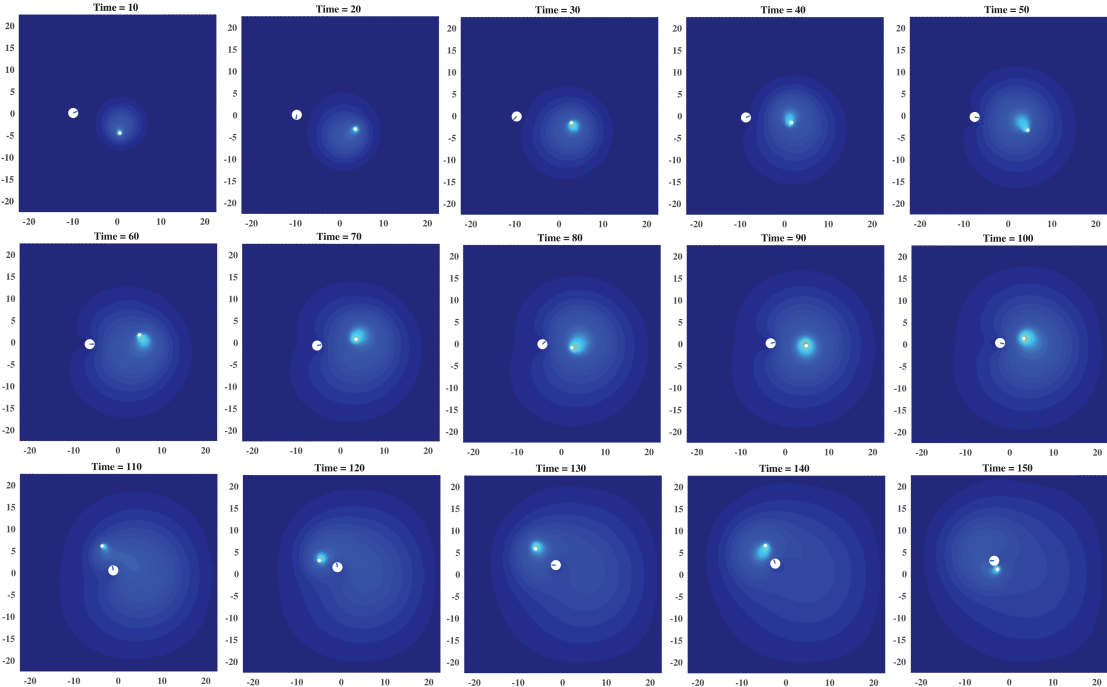


Figure F5: Time lapse snapshots of a typical simulation with $D = 1$, $\delta_J = 0.1$ and no bacterial rheotaxis. The color scale is the same as main figure 3C.

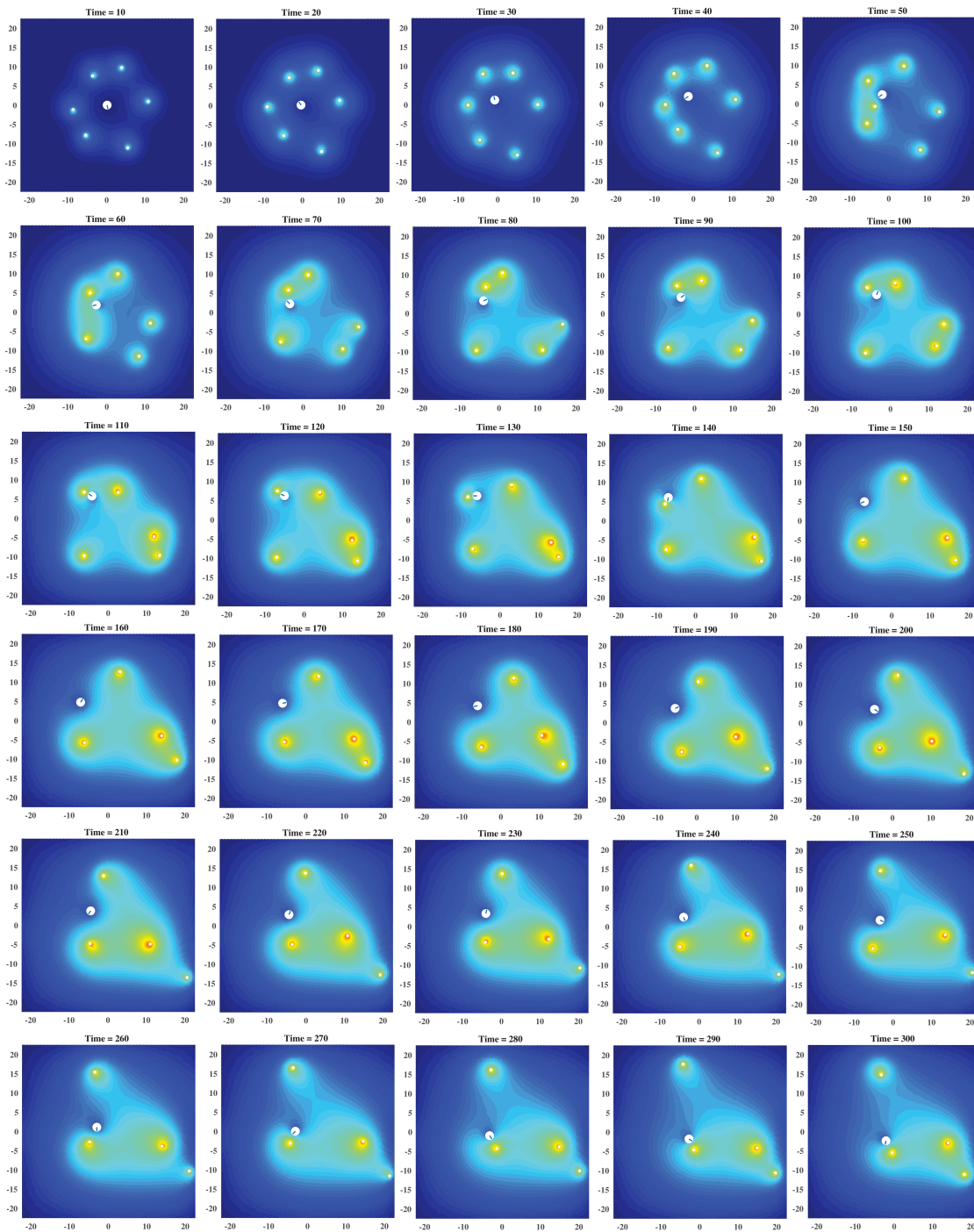


Figure F6: Time lapse snapshots of a typical simulation with 6 bacteria, $D = 1$, $\delta_J = 0.1$, no bacterial rheotaxis. The color scale is the same as main figure 3C.

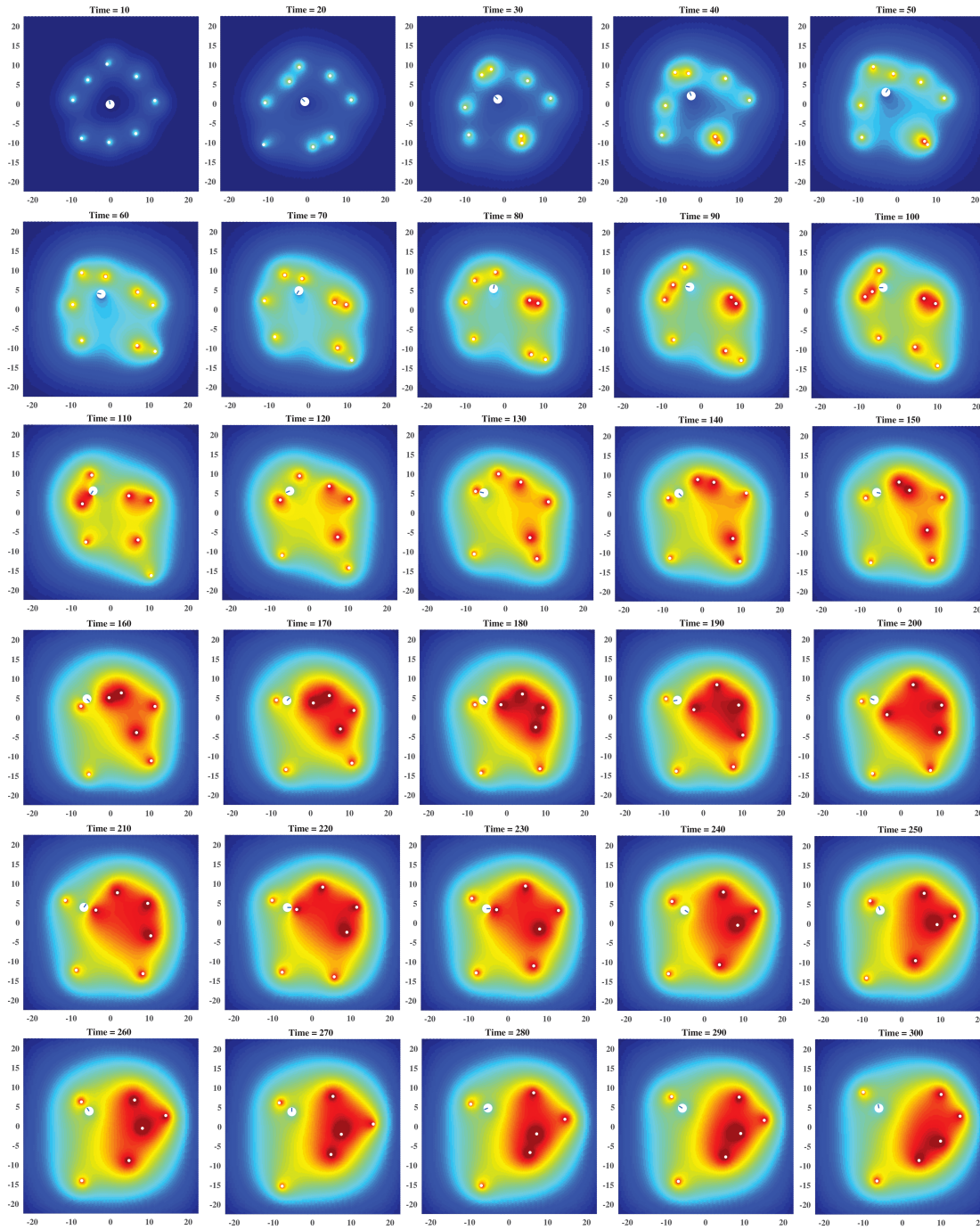


Figure F7: Time lapse snapshots of a typical simulation with 8 bacteria, $D = 1$, $\delta_J = 0.1$, no bacterial rheotaxis. The color scale is the same as main figure 3C.

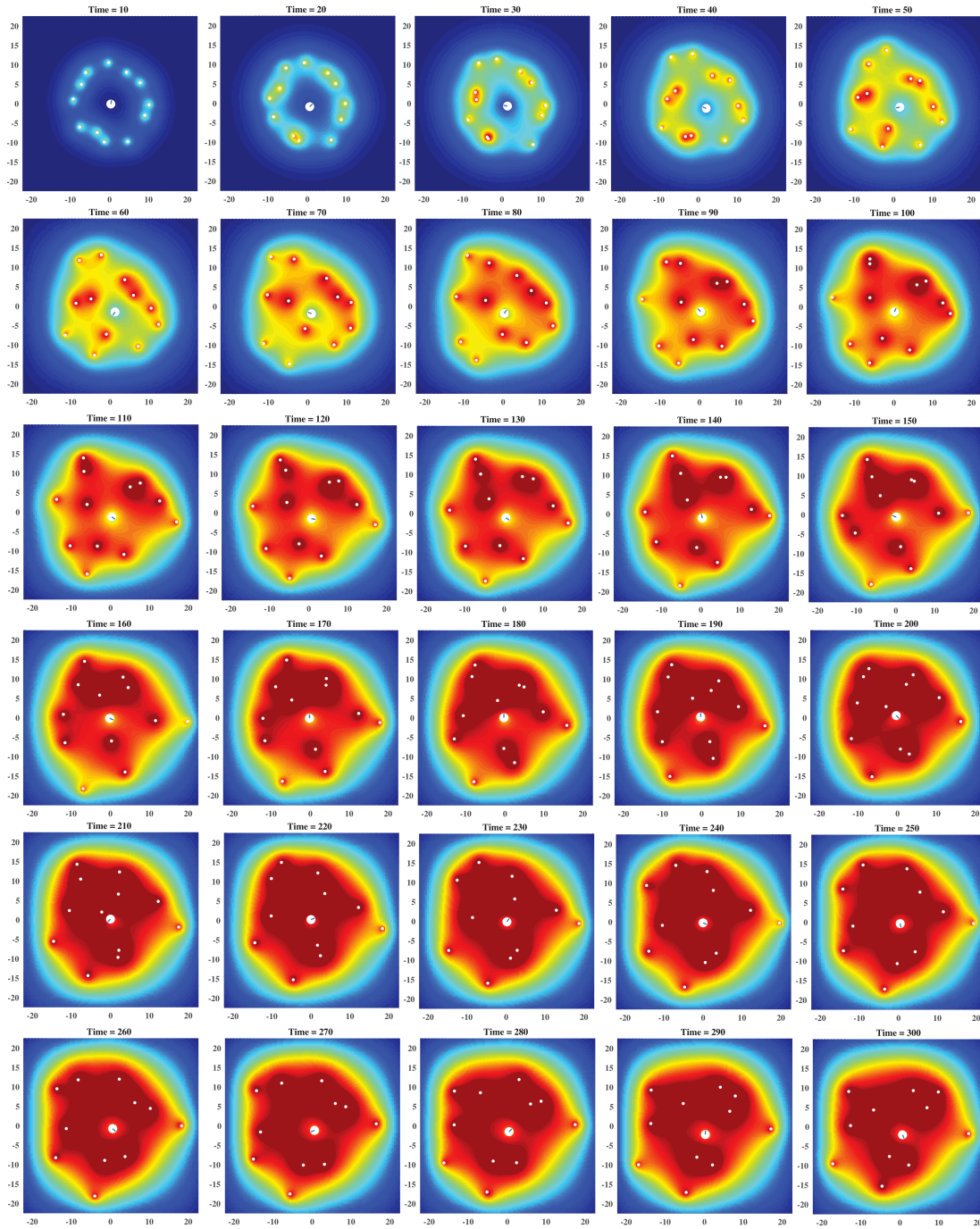


Figure F8: Time lapse snapshots of a typical simulation with 12 bacteria, $D = 1$, $\delta_J = 0.1$, no bacterial rheotaxis. The color scale is the same as main figure 3C.

References

- [1] Delanoë-Ayari H, Iwaya S, Maeda YT, Inose J, Riviere C, Sano M, Rieu JP 2008 Changes in the magnitude and distribution of forces at different *Dictyostelium* developmental stages *Cell. Motil. Cytoskeleton* **65**(4) 314-31

- [2] Sokolov A, Apodaca MM, Grzybowski BA, Aranson IS 2010 Swimming bacteria power microscopic gears *PNAS* **107(3)** 969-74
- [3] Riedel IH, Kruse K, Howard J 2005 A self-organized vortex array of hydrodynamically entrained sperm cells *Science* **309(5732)** 300-3
- [4] Lauga E, DiLuzio WR, Whitesides GM, Stone HA 2006 Swimming in circles: motion of bacteria near solid boundaries *Biophys. J.* **90(2)** 400-12
- [5] Rafai S, Jibuti L, Peyla P 2010 Effective viscosity of microswimmer suspensions *Phys. Rev. Lett.* **104(9)** 098102
- [6] Manahan CL, Iglesias PA, Long Y, Devreotes PN 2004 Chemoattractant signaling in Dictyostelium discoideum *Annu. Rev. Cell Dev. Biol.* **20** 223-53
- [7] Howe JD, Barry NP, Bretscher MS 2013 How do amoebae swim and crawl? *PLoS One* **8(9)** e74382
- [8] Bray D 2000 *Cell movements: from molecules to motility* (Garland Science)
- [9] Stewart RC, Dahlquist FW 1987 Molecular components of bacterial chemotaxis *Chem. Rev.* **87(5)** 997-1025
- [10] Block SM, Segall JE, Berg HC 1982 Impulse responses in bacterial chemotaxis *Cell* **31(1)** 215-26
- [11] Berg HC 1990 Bacterial microprocessing *Cold Spring Harbor symposia on quantitative biology* (Cold Spring Harbor Laboratory Press) p 539-545
- [12] Paluch E, Piel M, Prost J, Bornens M, Sykes C 2005 Cortical actomyosin breakage triggers shape oscillations in cells and cell fragments *Biophys. J.* **89(1)** 724-33
- [13] Tinevez JY, Schulze U, Salbreux G, Roensch J, Joanny JF, Paluch E 2009 Role of cortical tension in bleb growth *PNAS* **106(44)** 18581-6
- [14] Kay RR 2002 Chemotaxis and cell differentiation in Dictyostelium *Curr. Opin. Microbiol.* **5(6)** 575-9
- [15] Kessin RH 2001 *Dictyostelium: evolution, cell biology, and the development of multicellularity* (Cambridge University Press)
- [16] Bonner JT 2009 *The social amoebae: the biology of cellular slime molds* (Princeton University Press)
- [17] Devreotes PN, Zigmond SH 1988 Chemotaxis in eukaryotic cells: a focus on leukocytes and Dictyostelium *Annu. Rev. Cell Biol.* **4(1)** 649-86
- [18] Bonner JT 2015 *Cellular slime molds* (Princeton University Press)
- [19] Meinhardt H 1999 Orientation of chemotactic cells and growth cones: models and mechanisms *J. Cell Sci.* **112(17)** 2867-74
- [20] Neilson MP, Mackenzie JA, Webb SD, Insall RH 2011 Modeling cell movement and chemotaxis using pseudopod-based feedback *SIAM J. Sci. Comput.* **33(3)** 1035-57
- [21] Neilson MP, Veltman DM, van Haastert PJ, Webb SD, Mackenzie JA, Insall RH 2011 Chemotaxis: a feedback-based computational model robustly predicts multiple aspects of real cell behaviour *PLoS Biol.* **9(5)** e1000618
- [22] Hecht I, Skoge ML, Charest PG, Ben-Jacob E, Firtel RA, Loomis WF, Levine H, Rappel WJ 2011 Activated membrane patches guide chemotactic cell motility *PLoS Comput. Biol.* **7(6)** e1002044
- [23] Tang Y, Othmer HG 1995 Excitation, oscillations and wave propagation in a G-protein-based model of signal transduction in Dictyostelium discoideum *Philos. Trans. R. Soc. Lond., B, Biol. Sci.* **349(1328)** 179-95
- [24] Dallon JC, Othmer HG 1997 A discrete cell model with adaptive signalling for aggregation of Dictyostelium discoideum *Philos. Trans. R. Soc. Lond., B, Biol. Sci.* **352(1351)** 391-417
- [25] Palsson E, Othmer HG 2000 A model for individual and collective cell movement in Dictyostelium discoideum. *PNAS* **97(19)** 10448-53
- [26] Dallon JC, Othmer HG 2004 How cellular movement determines the collective force generated by the Dictyostelium discoideum slug *J. Theor. Biol.* **231(2)** 203-22
- [27] Khamviwath V, Hu J, Othmer HG 2013 A continuum model of actin waves in Dictyostelium discoideum *PLoS One* **8(5)** e64272
- [28] Cheng Y, Othmer H 2016 A model for direction sensing in Dictyostelium discoideum: Ras activity

- and symmetry breaking driven by a $G_{\beta\gamma}$ -mediated, $G_{\alpha 2}$ -Rac8-dependent signal transduction network *PLoS Comput. Biol.* **12(5)** e1004900
- [29] Bretschneider T, Othmer HG, Weijer CJ 2016 Progress and perspectives in signal transduction, actin dynamics, and movement at the cell and tissue level: lessons from Dictyostelium *Interface Focus* **6(5)** 20160047
- [30] Dallon JC, Othmer HG 1998 A continuum analysis of the chemotactic signal seen by dictyostelium discoideum *J. Theor. Biol.* **194(4)** 461-83
- [31] Wilhelm C, Riviere C, Biais N 2007 Magnetic control of Dictyostelium aggregation *Phys. Rev. E* **75(4)** 041906
- [32] Janney PA, McCulloch CA 2007 Cell mechanics: integrating cell responses to mechanical stimuli *Annu. Rev. Biomed. Eng.* **9** 1-34
- [33] Rivière C, Marion S, Guillén N, Bacri JC, Gazeau F, Wilhelm C 2007 Signaling through the phosphatidylinositol 3-kinase regulates mechanotaxis induced by local low magnetic forces in Entamoeba histolytica *J. Biomech.* **40(1)** 64-77
- [34] Décavé E, Rieu D, Dalous J, Fache S, Bréchet Y, Fourcade B, Satre M, Bruckert F 2003 Shear flow-induced motility of Dictyostelium discoideum cells on solid substrate *J. Cell Sci.* **116(21)** 4331-43
- [35] Holmes WR, Edelstein-Keshet L 2012 A comparison of computational models for eukaryotic cell shape and motility *PLoS Comput Biol.* **8(12)** e1002793
- [36] Van Haastert PJ 2011 Amoeboid cells use protrusions for walking, gliding and swimming *PLoS One* **6(11)** e27532
- [37] Barry NP, Bretscher MS 2010 Dictyostelium amoebae and neutrophils can swim *PNAS* **107(25)** 1376-80
- [38] Franz A, Wood W, Martin P 2018 Fat body cells are motile and actively migrate to wounds to drive repair and prevent infection *Dev. Cell* **44(4)** 460-70
- [39] Wang Q, Othmer HG 2016 Computational analysis of amoeboid swimming at low Reynolds number *J. Math. Biol.* **72(7)** 1893-926.
- [40] Wu H, Thiébaud M, Hu WF, Farutin A, Rafai S, Lai MC, Peyla P, Misbah C 2015 Amoeboid motion in confined geometry *Phys. Rev. E* **92(5)** 050701
- [41] Wu H, Farutin A, Hu WF, Thiébaud M, Rafai S, Peyla P, Lai MC, Misbah C 2016 Amoeboid swimming in a channel *Soft Matter* **12(36)** 7470-84
- [42] Aoun L, Farutin A, Garcia-Seyda N, Nègre P, Rizvi MS, Tlili S, Song S, Luo X, Biarnes-Pelicot M, Galland R, Sibarita JB 2020 Amoeboid swimming is propelled by molecular paddling in Lymphocytes *Biophys. J.* **119(6)** 1157-77
- [43] Dalal S, Farutin A, Misbah C 2020 Amoeboid swimming in a compliant channel *Soft Matter* **16(6)** 1599-613
- [44] Farutin A, Rafai S, Dysthe DK, Duperray A, Peyla P, Misbah C 2013 Amoeboid swimming: a generic self-propulsion of cells in fluids by means of membrane deformations *Phys. Rev. Lett.* **111(22)** 228102
- [45] Bouffanais R, Yue DK 2010 Hydrodynamics of cell-cell mechanical signaling in the initial stages of aggregation *Phys. Rev. E* **81(4)** 041920
- [46] Campbell EJ, Bagchi P 2017 A computational model of amoeboid cell swimming. *Phys. Fluids* **29(10)** 101902
- [47] Campbell EJ, Bagchi P 2020 A computational study of amoeboid motility in 3D: the role of extracellular matrix geometry, cell deformability, and cell-matrix adhesion *Biomech Model Mechanobiol* 1-25
- [48] Shapere A, Wilczek F 1987 Self-propulsion at low Reynolds number *Phys. Rev. Lett* **58(20)** 2051
- [49] Shapere A, Wilczek F 1989 Geometry of self-propulsion at low Reynolds number *J. Fluid Mech.* **198** 557-85
- [50] Avron JE, Gat O, Kenneth O 2004 Optimal swimming at low Reynolds numbers *Phys. Rev. Lett* **93(18)** 186001

- [51] Grossman N, Ron EZ, Woldringh CL 1982 Changes in cell dimensions during amino acid starvation of *Escherichia coli* *J. Bacteriol.* **152(1)** 35-41
- [52] Fu HC, Powers TR, Stocker R 2012 Bacterial rheotaxis *PNAS* **109(13)** 4780-5
- [53] Pan M, Neilson MP, Grunfeld AM, Cruz P, Wen X, Insall RH, Jin T 2018 A G-protein-coupled chemoattractant receptor recognizes lipopolysaccharide for bacterial phagocytosis *PLoS Biol.* **16(5)** e2005754
- [54] Cosson P, Soldati T 2008 Eat, kill or die: when amoeba meets bacteria *Curr. Opin. Microbiol.* **11(3)** 271-6
- [55] Bottino DC 2001 Computer simulations of mechanochemical coupling in a deforming domain: applications to cell motion *Mathematical Models for Biological Pattern Formation* (Springer, New York, NY) p 295-314
- [56] Dillon R, Owen M, Painter K 2008 A single-cell-based model of multicellular growth using the immersed boundary method *AMS Contemp. Math.*
- [57] Börgers C, Peskin CS 1987 A Lagrangian fractional step method for the incompressible Navier-Stokes equations on a periodic domain *J. Comput. Phys.* **70(2)** 397-438
466 1-5
- [58] Bae AJ, Bodenschatz E 2010 On the swimming of *Dictyostelium* amoebae *PNAS* **107(44)** E165-6
- [59] Muskhelishvili NI 2013 *Some basic problems of the mathematical theory of elasticity* (Springer Science & Business Media)
- [60] Cross MC, Hohenberg PC 1993 Pattern formation outside of equilibrium *Rev. Mod. Phys.* **65(3)** 851
- [61] Elliott CM, Stinner B, Venkataraman C 2012 Modelling cell motility and chemotaxis with evolving surface finite elements *J. R. Soc. Interface* **9(76)** 3027-44
- [62] Jana S, Um SH, Jung S 2012 Paramecium swimming in capillary tube *Phys. Fluids* **24(4)** 041901
- [63] Ledesma-Aguilar R, Yeomans JM 2013 Enhanced motility of a microswimmer in rigid and elastic confinement *Phys. Rev. Lett.* **111(13)** 138101
- [64] Sokolov A, Aranson I S, Kessler J O and Goldstein R E 2007 Concentration dependence of the collective dynamics of swimming bacteria *Phys. Rev. Lett.* **98** 158102
- [65] Lushi E, Goldstein R E and Shelley M J 2012 Collective chemotactic dynamics in the presence of self-generated fluid flows *Phys. Rev. E* **86** 040902
- [66] Lushi E, Goldstein R E and Shelley M J 2018 Nonlinear concentration patterns and bands in autochemotactic suspensions *Phys. Rev. E* **98** 052411
- [67] Nejad M R and Najafi A 2019 Chemotaxis mediated interactions can stabilize the hydrodynamic instabilities in active suspensions *Soft Matter* **11** 3248-55
- [68] Partridge J D, Nhu N T, Dufour Y S and Harshey R M 2019 *Escherichia coli* remodels the chemotaxis pathway for swarming *mBio* **10** e00316-19
- [69] Ryan SD 2019 Role of hydrodynamic interactions in chemotaxis of bacterial populations *Phys. Biol.* **17(1)** 016003
- [70] Xue C, Hwang HJ, Painter KJ, Erban R 2011 Travelling waves in hyperbolic chemotaxis equations. *Bull. Math. Biol.* **73(8)** 1695